AGU PUBLICATIONS

JGR

Journal of Geophysical Research: Planets

RESEARCH ARTICLE
10.1002/2013JE004557

Key Points:
- Two distinct units identified on ILD with unconformable contact
- Differences include layer thickness and mineralogy
- New geological model in the context of the history of Valles Marineris

Correspondence to:
F. Fueten,
ffueten@brocku.ca

Citation:
Fueten, F., J. Flahaut, R. Stesky, E. Hauber, and A. P. Rossi (2014), Stratigraphy and mineralogy of Candor Mensa, West Candor Chasma, Mars: Insights into the geologic history of Valles Marineris, *J. Geophys. Res. Planets*, *119*, doi:10.1002/2013JE004557.

Received 10 OCT 2013
Accepted 5 JAN 2014
Accepted article online 9 JAN 2014

Stratigraphy and mineralogy of Candor Mensa, West Candor Chasma, Mars: Insights into the geologic history of Valles Marineris

F. Fueten[1], J. Flahaut[2], R. Stesky[3], E. Hauber[4], and A. P. Rossi[5,6]

[1]Department of Earth Sciences, Brock University, St. Catharines, Ontario, Canada, [2]Faculty of Earth and Life Sciences, Vrije Universiteit Amsterdam, Amsterdam, Netherlands, [3]Pangaea Scientific, Brockville, Ontario, Canada, [4]Institute of Planetary Research, German Aerospace Center (DLR), Berlin, Germany, [5]International Space Science Institute, Bern, Switzerland, [6]Earth and Space Sciences, Jacobs University Bremen, Bremen, Germany

Abstract Candor Mensa, an interior layered deposit (ILD) in Valles Marineris, Mars, consists of two stratigraphically distinct units, the lower of which comprises the bulk of the mensa. This lower unit is approximately 5 km thick and composed of parallel layers, 4 to 14 m in thickness and associated with monohydrated sulfates. The lower unit is disconformably overlain by an upper unit composed of thinner ($<$ 3 m) layers with diagnostic polyhydrated sulfate signatures. The original extent of proto-Candor Mensa and its lower unit included neighboring Baetis Mensa. We suggest that the source material for both units is airborne dust or ash but that the depositional environment for the units differs. First, the lower unit was deposited during the subsidence of an enclosed water-filled basin. This basin/lake could have been frozen periodically, with freeze-thaw episodes possibly linked to Martian obliquity cycles. Erosion, including the potential action of glaciers, was able to remove large volumes of material out of the basin during the tectonism that produced the current geometry of Valles Marineris. Deposition of the upper unit postdates this event and took place in the absence of standing water at high elevation. Groundwater or snowmelt may have provided the water required for sulfate formation and deposit induration. We conclude that the major break in sedimentation recorded by this ILD deposit coincides with linking of ancestral basins into the current geometry of Valles Marineris chasmata and that it was possible to form hydrated minerals after this event.

1. Introduction

Valles Marineris, located on the eastern flank of the Tharsis region, is a 4000 km long linked system of up to 11 km deep troughs and has been the topic of numerous regional studies [e.g., *Frey*, 1979; *Tanaka*, 1986; *Lucchitta et al*., 1992; *Mège and Masson*, 1996; *Mège*, 2001; *Mège and Ernst*, 2001]. While Valles Marineris has been referred to as a rift [e.g., *Golombek and Phillips*, 2010], several studies [e.g., *Andrews-Hanna*, 2012a; *Mège and Masson*, 1996] suggested that only minor amounts of horizontal extension accompanied the vertical collapse. The formation of Valles Marineris is thought to have taken place during a two-stage process [*Lucchitta et al*., 1994; *Schultz*, 1998] of ancestral basin formation followed by the linking of the basins into their current geometry. Ancestral basins with irregular outlines, such as Hebes, Ophir, Candor, and possibly Melas Chasmata, were proposed to have formed prior to the opening of the Valles Marineris [*Lucchitta and Bertolini*, 1990; *Lucchitta et al*., 1994; *Malin and Edgett*, 2000, 2001]. The current geometry of Valles Marineris is generally considered to be a Hesperian structure [e.g., *Scott and Tanaka*, 1986; *Tanaka*, 1986; *Dohm and Tanaka*, 1999; *Head et al*., 2001; *Carr and Head*, 2010], though *Schultz* [1998] argued that a significant amount of faulting took place during the Amazonian.

Located within the chasmata of Valles Marineris are numerous enigmatic layered deposits, referred to as interior layered deposits (ILDs) [*Lucchitta et al*., 1994], whose origin and mechanism of formation are uncertain. *Lucchitta et al*. [1994] estimated that ILDs cover 17% of the total area, representing 60% by volume of all deposits within Valles Marineris. It has been suggested [*Catling et al*., 2006; *Malin and Edgett*, 2000] that ILDs are exhumed deposits, though most studies on ILDs conclude that they fill the early basins and are Hesperian deposits [e.g., *Scott and Tanaka*, 1986; *Tanaka*, 1986; *Schultz*, 1998; *Head et al*., 2001; *Carr and Head*, 2010]. ILDs have been proposed to have formed in lacustrine [*Nedell et al*., 1987] or aeolian [*Peterson*, 1981] environments; it has been also suggested that they are the result of pyroclastic volcanism in subaerial [*Hynek et al*.,

2003; *Chapman*, 2002; *Lucchitta*, 1987, 1990] or subglacial [*Nedell et al*., 1987; *Chapman and Tanaka*, 2001; *Komatsu et al*., 2004] environments. *Rossi et al*. [2008] suggested they are spring deposits, and *Kite et al*. [2013] suggested that seasonal snowmelt provided the liquid water for their formation. *Fueten et al*. [2008] argued that ILDs are deposited syntectonically during basin collapse with individual mounds being the remnants of filled subbasins.

Mineralogical data from both the OMEGA (Observatoire pour la Minéralogie, l'Eau, les Glaces et l'Activité; Mars Express (MEx)) [*Bibring et al*., 2004] and CRISM (the Compact Reconnaissance Imaging Spectrometer for Mars; Mars Reconnaissance Orbiter (MRO)) [*Murchie et al*., 2007] instruments suggest the presence of sulfates within Valles Marineris [*Gendrin et al*., 2005; *Quantin et al*., 2005; *Bishop et al*., 2009; *Murchie et al*., 2009a, 2009b; *Flahaut et al*., 2010a]. Sulfates have been associated with ILDs in most chasmata [*Gendrin et al*., 2005; *Quantin et al*., 2005; *Le Deit et al*., 2008; *Mangold et al*., 2008; *Flahaut et al*., 2010b]. *Chojnacki and Hynek* [2008] argued that no single sulfate formation mechanism can account for the range of settings in which sulfates have been found. However, it has been suggested that sulfates most likely formed in the presence of liquid water, under the acidic conditions of the Hesperian Epoch [*Bibring et al*., 2006; *Flahaut et al*., 2010a].

In this study we take advantage of newer HiRISE (High Resolution Imaging Science Experiment, MRO) [*McEwen et al*., 2007], CTX (Context Camera, MRO) [*Malin et al*., 2007], CRISM, and HRSC (High Resolution Stereo Camera, MEx) [*Neukum et al*., 2004] data to study the geology of Candor Mensa and its relationship with Baetis Mensa, two large ILDs within Candor Chasma (Figure 1). The goal is to gain a better understanding of their depositional and erosional histories. Because of the availability of data, the primary focus of this work is Candor Mensa.

2. Methodology

2.1. Imagery and Measurements of Layer Attitudes and Thickness

A mosaic of HRSC images and digital elevation models (DEM) from MEx orbits 334 and 360 formed the base map for this study. CTX images were registered to this base map. HiRISE images, rescaled to 1 m/pixel, were then registered to the CTX images. The intermediate step of registering the CTX images was deemed necessary to ensure proper registration of the HiRISE images to the HRSC DEM. Layer thickness data were obtained by measuring layer intersects along the rescaled HiRISE images. To ensure that no layer was missed in the rescaled images, the full-resolution HiRISE image was available for checking in a secondary monitor. Layer intersection measurements were taken along multiple transects of 200 m in length, aligned parallel to the slope of the wall. Layers were only counted along a transect in which no portion was covered by dunes or obscured due to image illumination issues. The attitude of the wall slope, the mean elevation of the transect, and, where possible, the attitude of the layering were recorded. Because the resolution of the underlying DEM varied from 50 m/pixel to 100 m/pixel, only a single average layer thickness was calculated for each transect. Layer attitudes were measured with the software program Orion [*Fueten et al*., 2008], and the average thickness was, where possible, corrected for the apparent dip. Since layer dip values in all cases were less than 10°, apparent dip correction resulted in average thickness changes of less than 1 m.

All available HiRISE images were examined, but only seven HiRISE images of Candor Mensa contained regions that had sufficiently clean outcrops for us to feel confident that we could measure every layer along transects. We found no suitable locations on any HiRISE images of Baetis Mensa. Since our data are acquired along numerous short transects, we did not attempt a frequency analysis and hence have no information on cyclicity as found by *Lewis et al*. [2008].

To test the accuracy of this transect method, two HiRISE DEM, one for the lower unit and one for the upper unit, were constructed using the NASA Stereo Pipeline [*Moratto et al*., 2010; *Broxton and Edwards*, 2008]. To ensure that the elevations of both HiRISE DEMs were compatible with the elevations of the HRSC transects, the elevation of the HiRISE DEM were offset to match the elevations of the HRSC DEM. Within these images, the thickness of individual layers could be measured in the same locations as transects and the values of the two methods could be compared. Results of this test will be discussed in detail below.

2.2. Mineral Identification

Hyperspectral observations from CRISM were used to determine the mineralogy of the deposits when available. With full spatial and spectral resolution, CRISM can collect data at 18 m/pixel over 544 channels

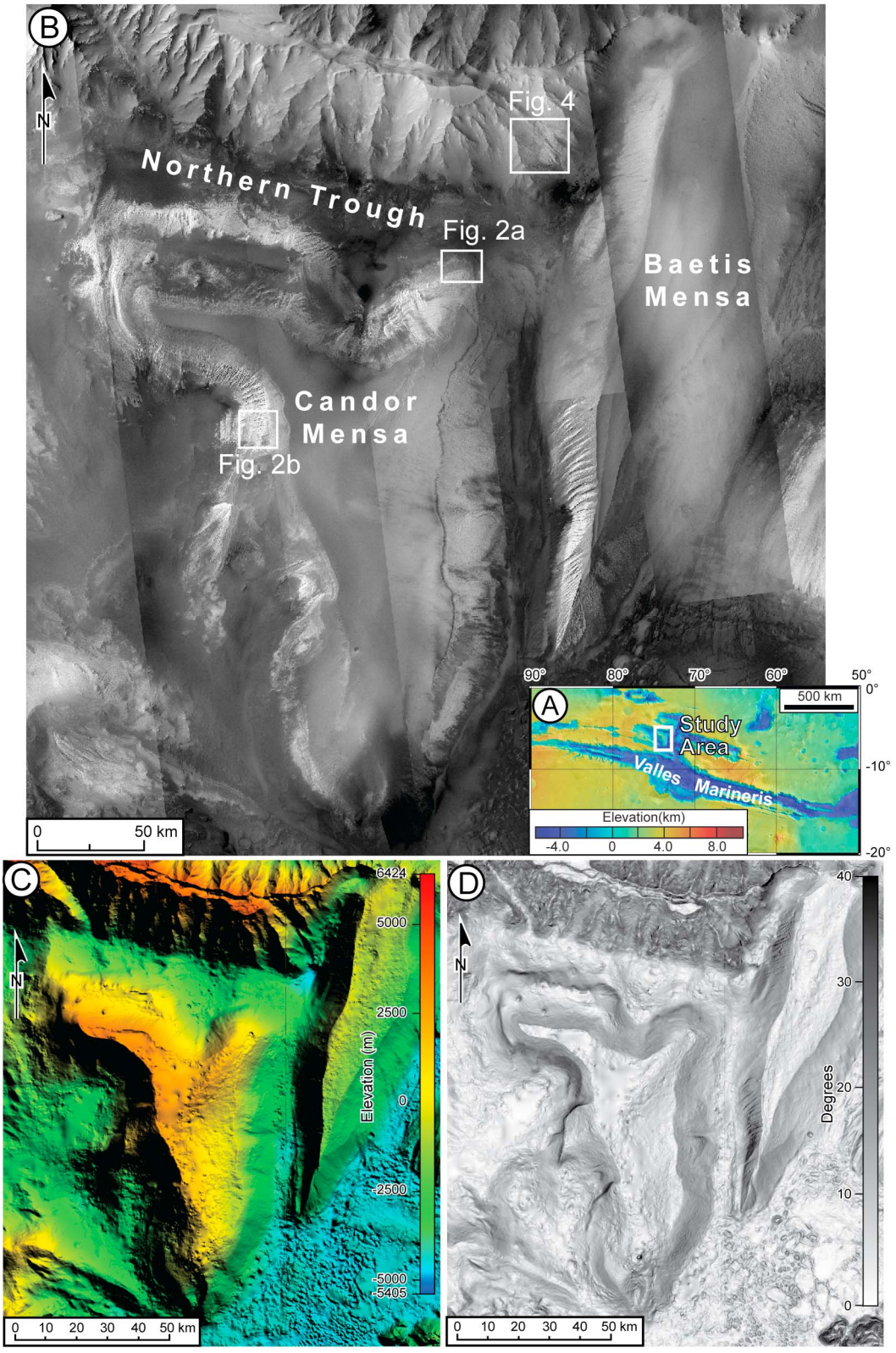

Figure 1. (a) Location of Candor and Baetis Mensae. (b) CTX Mosaic with locations for Figures 2 and 4 as indicated. (c) Digital elevation model based on HRSC data from orbits 360 and 334. (d) HRSC slope map.

from 362 to 3920 nm at 6.55 nm/channel sampling [*Murchie et al*., 2007, 2009c], over a scene of approximately 10 km by 10 km in size. Atmospheric and photometric corrections were implemented as described by *Mustard et al*. [2008] and *Murchie et al*. [2009c] using the CRISM Analysis Tool (CAT) for ENVI software. Noise-removal algorithms, such as the destriping and despiking functions from CRISM Iterative Recognition and Removal of Unwanted Spiking (CIRRUS) [*Parente*, 2008], were implemented in the case of Targeted Reduced Records v. 2 data before projection. Spectra were extracted from regions of interest on the basis of spectral parameter maps [*Pelkey et al*., 2007] commonly using a 3×3 pixel average. Residual artifacts after calibration and atmospheric removal are suppressed by ratioing the spectra to a spectrally neutral region in the same detector column. CRISM spectra obtained were finally compared with reference spectra of terrestrial samples present in the CAT spectral library.

3. Geology of Candor Mensa

Candor Mensa (Figure 1) is one of the largest free-standing ILDs within the Valles Marineris trough system. It measures approximately 70 km east to west along its northern limit and extends approximately 115 km from north to south. The best estimate for the elevation of the floor of the local chasma is ~ −4700 m to −4300 m (Figure 1c), and within the CTX images (of ~6 m/pixel resolution), layering can be detected at elevations as low as −4700 m in the north and at −4500 m near the southern tip of Candor Mensa. With a peak at ~3360 m, Candor Mensa can, to a first approximation, thus be described as an 8 km high ILD deposited on a level floor [*Fueten et al*., 2011a]. Located immediately to the east of Candor Mensa is Baetis Mensa, which is separated from Candor Mensa by a narrow straight channel (Figure 1).

Light-toned layered material, exposed along the flanks of Candor Mensa (Figure 1), appears to be fresh and is essentially devoid of craters. Along some portions of the flanks, the material is heavily fluted with well-developed yardangs [e.g., see *Chojnacki and Hynek*, 2008, Figure 10e; *Lucchitta*, 1999]. These flutes and well-developed layering are primarily visible along the western and northern extents of the deposit. Layering in some locations appears as alternating dark and light bands within CTX images. However, HiRISE images illustrate that the dark material is a later deposit covering the outcrops of light-colored benches.

A major erosional bench at an elevation of ~2000 m (local top elevation ~3100 m) can be traced around the northwest promontory of Candor Mensa. This elevation approximately coincides with the upper extent of the major yardangs located along the western side of Candor Mensa. Layering immediately above the bench and visible within CTX images can be traced around the lobe. Layer attitude measured with a trace length of 30 km indicates that layering dips 2° to the NW. Generally all layering measured within Candor Mensa is shallow, dipping less than 10°.

The eastern flank of Candor Mensa is a relatively featureless planar surface of light-toned material. In a few locations, features are found that may be interpreted as poorly exposed layering outcrop and, in at least one area, poorly developed flutes. The slope of this side of Candor is generally shallow and decreases from ~25° at the southern tip to ~12° near the northern extent of Candor Mensa.

Multiple parallel fractures forming fracture sets were observed at all elevations in several locations. No fractures filled with resistant material, as described by *Okubo* [2010], were observed. In some locations fractures offset layers, but the true sense of offset is unknown. Along the western side of the mound a major scarp, which will be described in more detail below, has been mapped by *Lucchitta* [1999] as a normal fault.

Candor Mensa is capped by a fairly uniform, dark, smooth, and resistant layer [*Lucchitta*, 1999; unit AHire]. According to *Lucchitta* [1999], this unit also caps several adjacent ILDs, such as Baetis Mensa and the ILD in East Candor Chasma. This unit appears to be broken by minor scarps along the top of Candor Mensa. In appearance, similar dark capping material can also be found as small patches covering the slopes of Candor Mensa. The aerial extent over which this capping unit has been observed makes it an interesting geological feature; it clearly postdates the bulk of the geological history investigated here.

Aside from the thin late capping unit, Candor Mensa can be broadly divided into two major units on the basis of stratigraphy, layer morphology, and mineralogy.

3.1. Lower Unit

No basal contact of the lower unit with another lithology was found. The lowest outcrops of layered material (elevation ~ −2200 m) on the northeast end of Candor Mensa (Figure 2a) belong to this unit. The upper

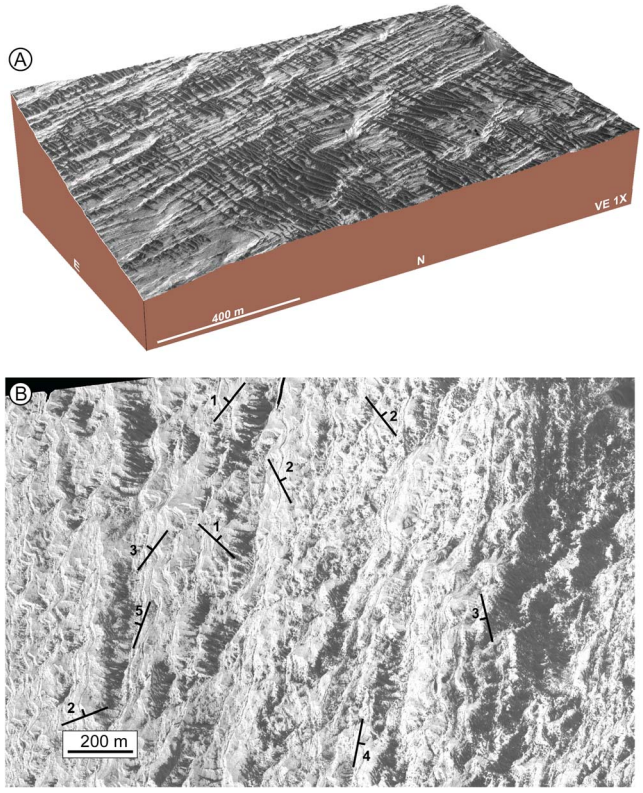

Figure 2. Lower unit, locations in Figure 1. (a) (Images PSP_009038_1745 and PSP_010027_1745) 3-D view of nearly horizontal continuous layering. (b) (Images PSP_004186_1740 and PSP_005597_1740) Layering measured using the HiRISE DEMs calculated with the NASA Ames Stereo pipeline [*Moratto et al*., 2010; *Broxton and Edwards*, 2008] and Orion software (© Pangaea Scientific) [*Fueten et al*., 2008] indicates that the layering in both locations dips less than 5°.

boundary of this unit, with the exception discussed below, cannot clearly be defined. In many locations, such as the northeast end, it appears to extend directly underneath the capping unit at an elevation of nearly 3000 m. Layering is subhorizontal, with dips of less than 5°. Since outcrops of this unit can be continuously traced from the lowest to the highest elevations of the mound along the northern edge, at least 5 km of continuous stratigraphy can be traced along the northern side of Candor Mensa.

Komatsu et al. [1993, Figure 10] described benches on the western side of Candor Mensa and suggested that major fluting coincides with approximately the same stratigraphic level as those benches. We are unable to demonstrate that these features coincide with any particular stratigraphic level; both are located within our lower unit.

Two representative locations with stereo HiRISE images and distinct layering, one near the northeast end (Figure 2a) and one near the western central portion (Figure 2b) of the ILD, were chosen to examine this unit in more detail. In both locations, individual layers could be traced for several kilometers. Larger benches covered with dunes crop out. These dunes are responsible for the alternating light and dark morphology observed in lower resolution imagery. In some cases additional layer boundaries are visible between the benches. No angular unconformities or localized thickness variations (e.g., channels) were observed anywhere.

3.2. Upper Unit

Outcrops of the upper unit can be visually identified only along the western edge of Candor Mensa, where its base coincides with the base of a cliff (Figure 3). Three separate outcrops of this cliff can be identified (Figure 3a). The cliff material itself is composed of upper unit (Figures 3b and 3c). The geometry of the base of the cliff and thus the nature of the contact between units is discussed in more detail below.

The erosion pattern of the cliff differs from that of the lower unit. Downslope-trending narrow ridges dominate the outcrop pattern of the cliff, rather than the layer parallel benches exhibited by the lower unit.

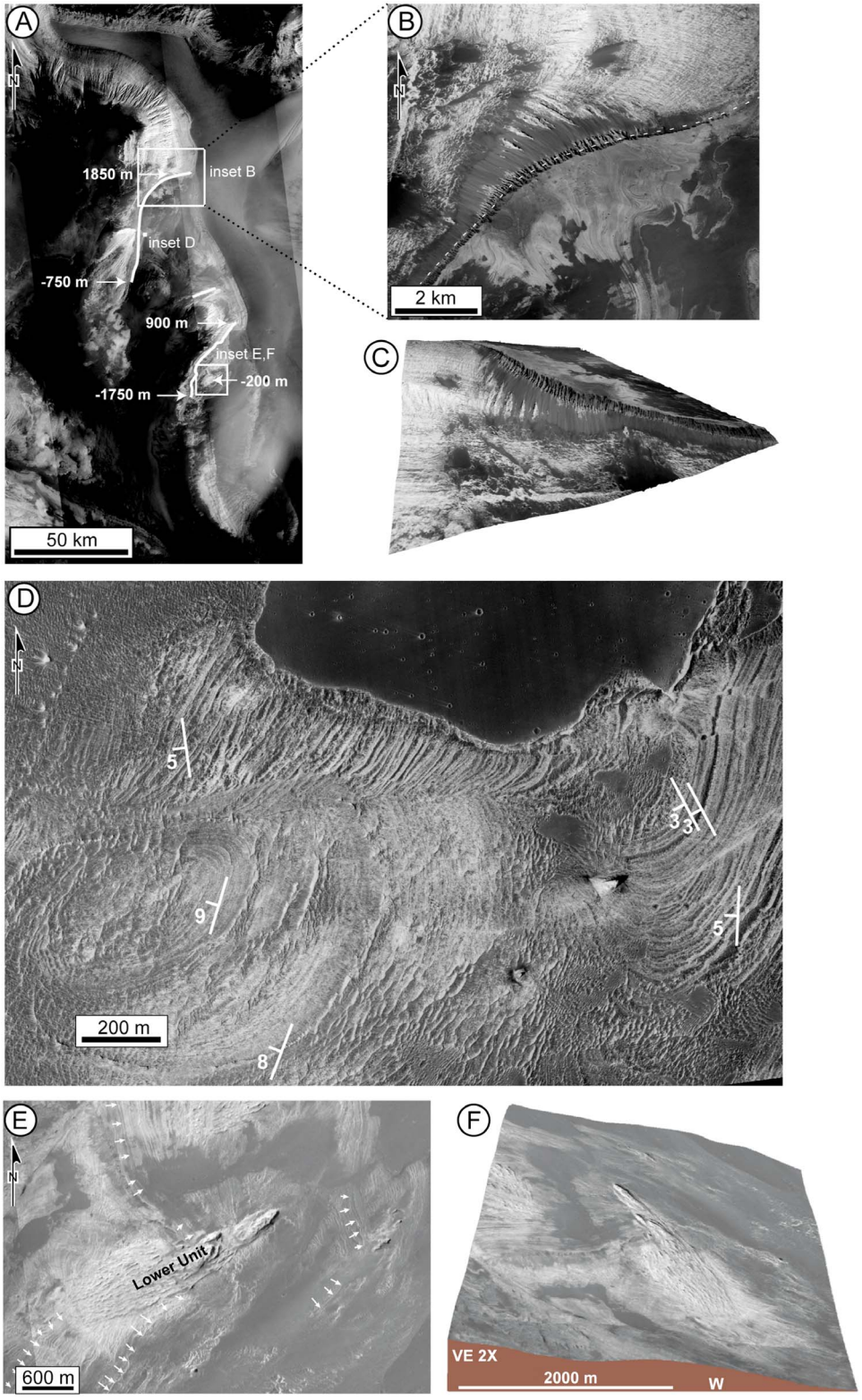

Figure 3. (a) Locations of cliffs (white lines) along west side of Candor Mensa visible in CTX mosaic. Elevations as marked. (b) Detailed view of cliff. Light-toned material north of the cliff is part of the lower unit. The cliff and the material south of the cliff compose the upper unit (P15_006955_1745_XI_05S073W). (c) 3-D view of Figure 3b, indicating that contact cuts across near horizontal lower unit. (d) Dips of upper unit measured from HiRISE Stereo DEM (PSP_004186_1740/ PSP_005597_1740). Several fractures offset layers, especially near the NE corner of the image. (e, f) Layering of upper unit displayed by arrow (P15_006955_1745_XI_05S073W). Outcrop of what is interpreted as lower unit is indicated. Note that the upper unit layering is interrupted by the outcrop of lower/older unit, elevated above upper/younger unit layering.

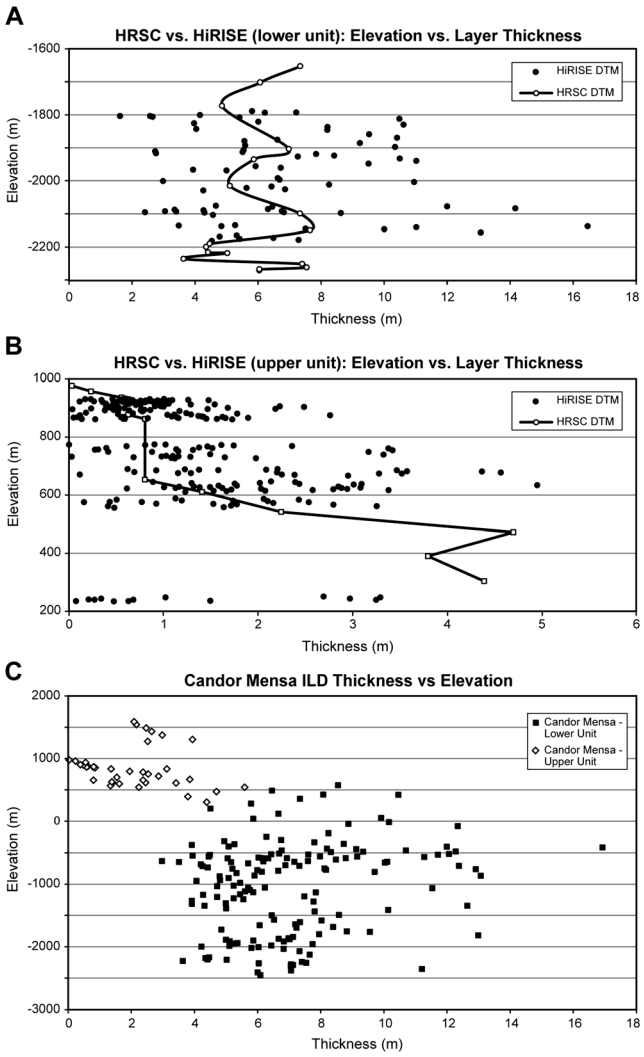

Figure 4. (a) Direct HiRISE DEM-based bed thickness measurements (images PSP_009038_1745 and PSP_010027_1745) versus HRSC DEM-based transect measurements for lower unit. (b) Direct HiRISE DEM-based bed thickness measurements (images PSP_004186_1740 + PSP_005597_1740) versus HRSC DEM-based transect measurements for upper unit. (c) HRSC DEM-based transect measurement for upper and lower units. Note the difference in bed thicknesses.

Fractures with offsets (Figure 3d) indicate that the upper unit is consolidated and the presence of the cliff itself indicates that it is more competent than the lower unit. Layering of the upper unit is on a finer scale than that of the lower unit and exhibits no bench morphology. No angular unconformities or localized thickness variations were observed in the upper unit. Even though fracturing has clearly disrupted the layering in some locations (Figure 3d), the layers themselves appear to be parallel to each other. Unfortunately, the dip of the upper unit could only be reliably measured within an outcrop that also contains fractured layers (Figure 3d). Dips are between 3° and 9° (Figure 3d), where some of the variability in dip is likely the result of the fracturing.

In the location of the cliff, the upper unit is directly overlain by the thin resistant capping layer. This capping unit covers most of the top of Candor Mensa and is in direct contact with the lower unit in other locations. Thus, the true thickness of the upper unit is unknown, although it is at least 300 m, the maximum currently observed.

3.3. Nature of the Contact Between Units

Along both the longer northern and shorter southern sections of the cliff (Figure 3a), the elevation changes by about 2.6 km. Where it can be measured, the plane of contact varies in dip from 14° to 18°. In one location

near the southern portion of the contact, lower unit material forms an inlier, surrounded by an outcrop of the upper unit (Figures 3e and 3f). Since the layering in both units is nearly horizontal and the contact between them is not, the contact between the units is disconformable.

3.4. Layer Thickness Measurements

For the lower unit 17 transect measurements based on HRSC DEMs were compared to 74 direct layer measurements using the HiRISE DEM. Direct layer measurements indicate that visible layer thickness varies primarily between 2 m and 11 m (Figure 4a), with a few layers reaching thicknesses of approximately 16 m. Transect layer measurements, which provide an average, fall within the middle of the range of the direct measurement and as expected show less variation in thickness. The average thickness of directly measured layers using the HiRISE DEM of 6.7 m compares well with an average thickness of 6.8 m measured using the transect method.

For the upper unit, 14 transect measurements based on HRSC DEMs were compared to 246 direct HiRISE measurements (Figure 4b). The data indicate thicknesses of generally less than 4 m for both methods, indicating that the layers in the upper unit are thinner than those of the lower unit.

In total 191 HRSC DEM-based transect measurements were performed within 7 different HiRISE images and 11 separate locations (Figure 4c). Data indicate that lower unit thicknesses are generally in the 4 m to 13 m range, with the largest concentration between 4 m and 8 m. Data for the lower unit were collected over an elevation range of approximately 3 km which, since the layering is essentially horizontal, corresponds to a stratigraphic thickness of approximately 3 km. No coarsening or thinning trends are apparent over that range.

Transect thickness measurements of the upper unit are consistently less than those of the lower unit. There is a possible weak trend of layer thickness decreasing with increasing elevation within the lowest section of the upper unit.

4. Mineralogy of Candor Mensa

4.1. Previous Mineralogical Studies

Major aspects of the ILDs' composition were revealed by OMEGA and TES (Thermal Emission Spectrometer, Mars Global Surveyor). OMEGA detected the presence of hydrated sulfate minerals, often mixed with crystalline ferric oxides, in the ILDs of Valles Marineris [*Gendrin et al*., 2005; *Mangold et al*., 2008; *Le Deit et al*., 2008]. TES also detected patches of coarse-grained gray hematite in the vicinity of some ILDs, such as Candor Mensa [*Christensen et al*., 2001; *Weitz et al*., 2008].

Mangold et al. [2008] showed that Candor Mensa presents a characteristic mineralogic assemblage, with dominating Mg-rich monohydrated sulfates (kieserite) signatures mixed with nanophase ferric oxides signatures. Polyhydrated sulfates, of undefined cationic composition, were also detected more locally, in troughs between the mensa's northern flanks and the chasma wall, generally at low elevations (Figure 5). By contrast, kieserite is found mainly on heavily eroded scarps of light-toned material (Figure 5). Strong signatures of iron oxides are present on these sulfate-rich scarps and at the base of layered deposits. They appear to be correlated with a TES gray hematite signature and might correspond to material transported down the scarp [*Mangold et al*., 2008; *Weitz et al*., 2008].

A more recent survey by *Murchie et al*. [2009b] confirms these detections with CRISM data. This data set is used hereafter to precisely identify and map the different spectral signatures and characterize the mineralogical variations between different sets of layers.

4.2. Identification of Spectral Signatures

All of the CRISM hyperspectral data available over the study area were processed (Figure 5). Three main spectral types were identified by investigating the overtones and combinations of fundamental vibrational absorption features in the 1.0–2.6 μm interval, where key water absorptions are. All spectral types present a 2.4 μm feature which is common to all sulfates and characterizes the SO_4 group vibrations within the structure [*Gendrin et al*., 2005; *Cloutis et al*., 2006; *Bishop et al*., 2009]. The presence of ferric oxides and crystalline hematite was also inferred from wide absorptions in the 0–1 μm domain, generally triggering a drop in reflectance at wavelengths lower than 1.3 μm [*Clark et al*., 1987; *Bibring et al*., 2007]. These minerals are observed in association with the sulfates as discussed in the next section.

The first spectral type presents strong absorption bands at 2.1 and 2.4 μm and has been found in all the CRISM observations targeted over the ILDs (red and purple spectra in Figure 6d). The shift of the common bound water

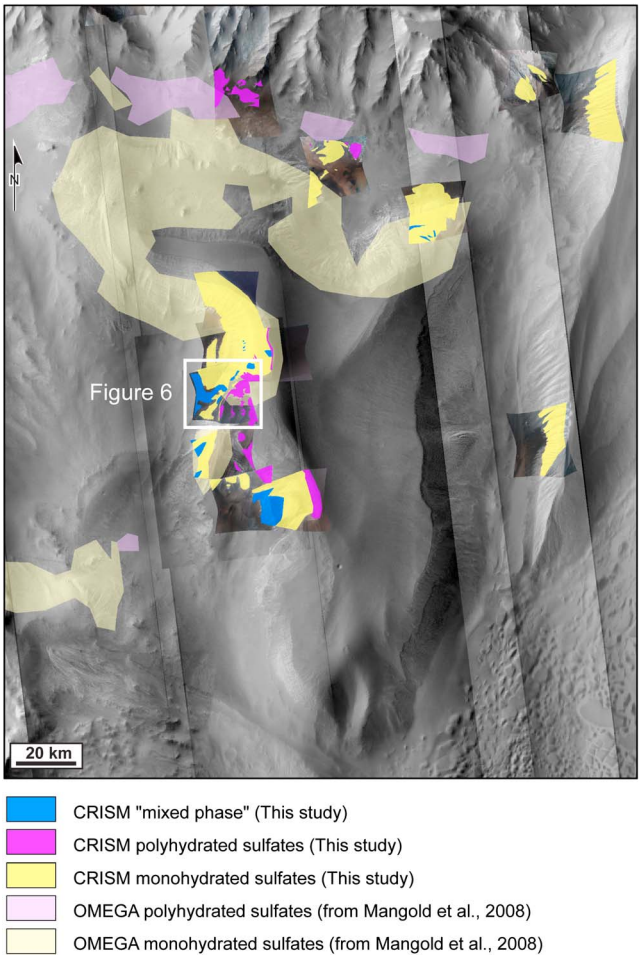

Figure 5. Hydrated minerals distribution as seen by CRISM (this study) and OMEGA [from *Mangold et al.*, 2008]. Monohydrated sulfates appear in yellow, polyhydrated sulfates in purple, and our mixed phase in blue. Background: CTX mosaic.

vibration from 1.9 to 2.1 μm in these spectra indicates the presence of a single water molecule in the sulfate structure. The combination of these two absorption features is diagnostic of monohydrated sulfates [*Gendrin et al.*, 2005; *Bibring et al.*, 2005]. The doublet shape of the 2.1 μm band, the position of its minimum reflectance at 2.13 μm, and the general shape of the spectra are consistent with Mg-monohydrated sulfates such as kieserite ($MgSO_4$, H_2O) (Figure 8e) [*Gendrin et al.*, 2005; *Mangold et al.*, 2008]. Additional decreases in reflectance with decreasing wavelengths toward 1 μm correspond to the ferric mineral absorption in the visible domain. Both nanophase ferric oxides and crystalline ferric minerals are actually detected in association with monohydrated sulfates due to wide absorptions around 0.53 and 0.85 μm for the nanophase ferric oxides and 0.9 for the crystalline ferric minerals. Hematite is also identified by its 0.5 μm, 0.67 μm, and 0.86 μm set of absorptions (Figures 6b and 6d).

The second spectral type is characterized by a 1.4 μm, 1.94 μm, and 2.4 μm set of absorptions (green spectra, Figure 6d). Although the 1.4 μm and 1.9 μm absorption bands occur in all minerals containing H_2O [*Clark et al.*, 1990], the exact position of the 1.9 μm band and the coupling of this band with a 2.4 μm band is diagnostic of polyhydrated sulfates [*Gendrin et al.*, 2005; *Bishop et al.*, 2009]. The cationic composition of such sulfates is difficult to resolve with spectroscopic data. Some particular species such as Ca sulfates (gypsum, bassanite) can still be ruled out as they should present strong additional bands (e.g., 1.75 μm) in their spectra. Jarosite, which is expected to have strong absorptions at 1.85 and 2.27 μm, is also not a good candidate as these features are not observed and cannot explain the 1.9 μm band. Epsomite ($MgSO_4$, $7H_2O$) or melanterite ($FeSO_4$, $7H_2O$) are good candidates, but mixtures of several species are also plausible (Figure 8e). Ferric oxides are also contributing to the final spectral signature in the visible domain through their absorptions around 0.5 μm and 0.85 μm.

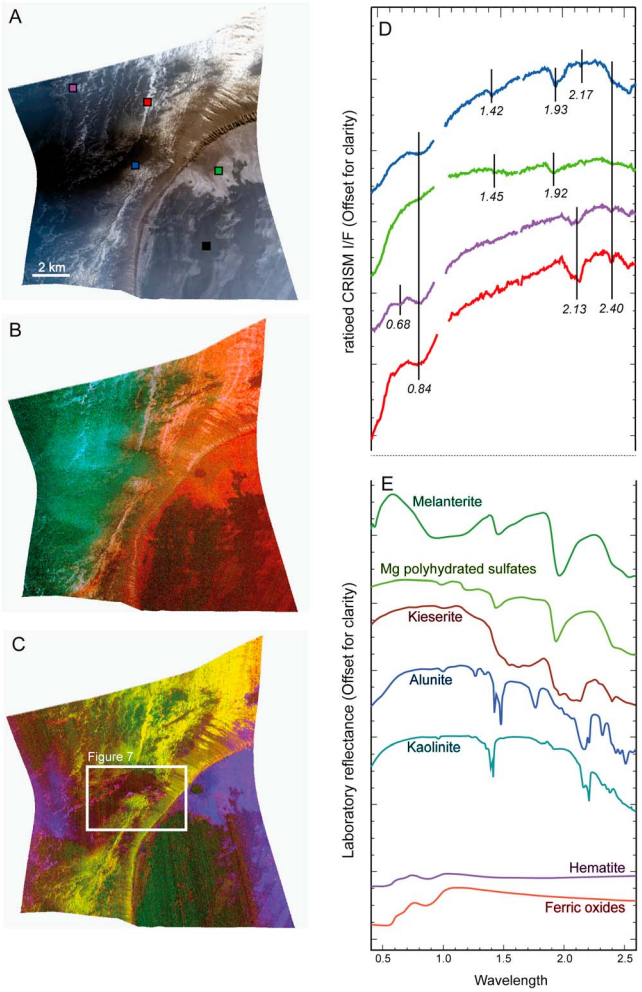

Figure 6. (a–d) Mineralogy of Candor Mensa as seen on CRISM observation FRT00006470. In Figure 6a, CRISM VNIR (visible and near-infrared) observation false color composition ($R = 0.7097$ μm, $G = 0.5989$ μm, and $B = 0.5337$ μm). In Figure 6b, RGB composition of VNIR summary parameters: R = BD530 (stretched values: 0.068–0.17), G = BD920 (stretched values: 0–0.03), and B = BD860 (stretched values: 0–0.013). Hematite-rich areas appear in cyan, whereas ferric oxide-rich areas appear in yellow/orange and crystalline ferric minerals in green. In Figure 6c, RGB composition of IR summary parameters: R = SINDEX (2.4 band, stretched values: 0.01–0.045), G = BD2100 (stretched values: 0.003–0.043), and B = BD1900R (stretched values: 0.001–0.016). PHS (polyhydrated sulfate)-rich areas (including the mixed phase) appear in purple, whereas MHS (monohydrated sulfate)-rich areas appear in yellow. In Figure 6d, CRISM ratioed spectra (the pixels used are shown with similar colors in Figure 6a). Line markings indicate the main absorptions. Channels involved in the common 1.65 μm artifact due to the detector boundary in CRISM spectra [*Murchie et al.*, 2007] have been masked for clarity. (e) Best library spectral matches are given for comparison.

The last spectral type shows diagnostic features at 1.44–1.45 μm, 1.93–1.94 μm, and 2.4 μm (blue spectra, Figure 6d). A weak additional band seems present at 2.17 μm (sometimes 2.20 μm), and a strong decrease in reflectance is observed from 2.3 μm to 2.5 μm. Although the main absorptions in this spectrum are those of a polyhydrated sulfate, no sample in the library can account for all of these features, making a mixture of two or more minerals more likely. The 2.17 μm spectral feature corresponds to the vibration of Al-OH bonds and is present in the reference spectra of Al-rich clays such as kaolinite or Al-rich sulfates such as alunite [*Clark et al.*, 1990; *Mustard et al.*, 2008; *Bishop et al.*, 2009]. In hydrated silicates 2.20 μm features might also be caused by Al-OH or Si-OH bonds but could also be created by the ratioing process if a monohydrated sulfate is present in the denominator. The 2.17 μm absorption is definitively an absorption band as it is also observed in raw CRISM spectra. Kaolinite should also present additional absorptions at 1.40 μm and 1.91 μm, whereas alunite should also present additional weak absorptions at 1.44 μm and 1.76 μm (Figure 8e). Such features are not observed in the spectra, but in the case of alunite they should be weaker than the 2.17 μm feature and could probably not be distinguish from the background noise. Common clay absorptions at 1.40 μm and 1.91 μm might also be masked or shifted by the presence of sulfates in the mixture [*Stack and Milliken*, 2011; *Noe Dobrea et al.*, 2012].

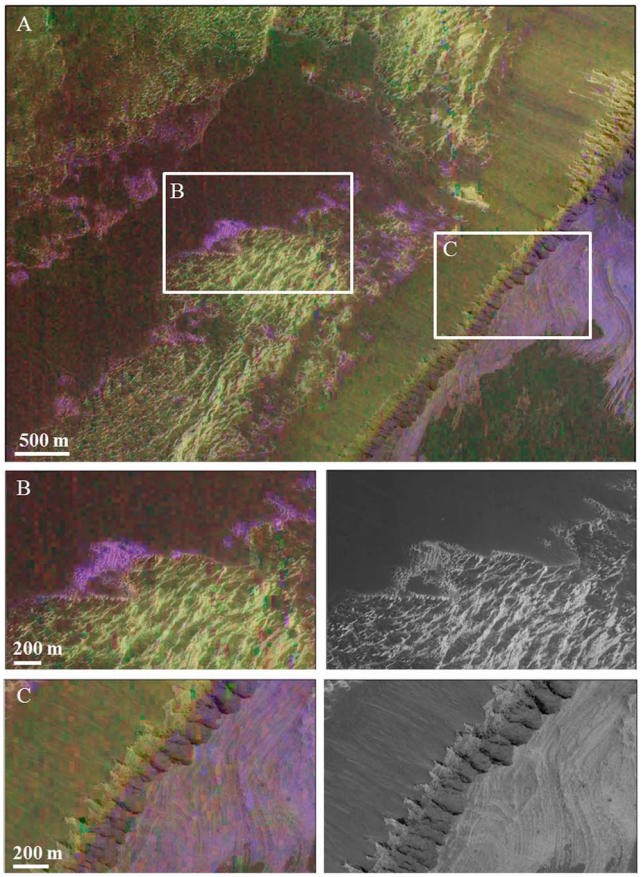

Figure 7. Previous mineralogic detections derived from the summary parameters map in Figure 6c are overlain on HiRISE PSP_004186_1740. (a) PHS-rich areas (including the upper unit PHS and the mixed phase) appear in purple tones and are identified over the edge of the capping layer and in the upper unit, whereas the lower unit seems dominated by MHS, represented in yellow. (b) Close-up on the capping layer edge, where our mixed phase is always detected. (c) Close-up on a portion of the upper unit, where PHS are detected.

We therefore cannot conclude on the nature of the Al-rich phase which is responsible for the 2.17 μm absorption. The strong decrease in reflectance observed in the spectrum between 2.3 μm and 2.5 μm is also present in some magnesian polyhydrated sulfates, such as starkeyite ($MgSO_4$, $4H_2O$) [*Bishop et al.*, 2009]. We therefore suggest that the third spectral type described here, referred to as a "mixed phase" throughout this paper, is likely a mixture of polyhydrated sulfates (including starkeyite) with an Al-rich mineral.

4.3. Mineralogical Distribution

The aforementioned detections are associated with different materials that coincide, for two of the spectral types, with the previously described stratigraphic units. These spectral types correspond to dominant mineralogies, but mixtures of several minerals are observed in many cases and are likely widespread among the area. Figures 5 and 6b show that monohydrated sulfates are detected in the lower unit of Candor Mensa. Monohydrated sulfates are also detected over the western flank of Baetis Mensa (Figure 5) and over the small outcrop of light-toned deposits located in the northern wall between Candor and Ophir Chasmata depicted in Figure 4.

As already noticed by many authors [*Quantin et al.*, 2005; *Mangold et al.*, 2008; *Flahaut et al.*, 2010a, 2010b], in other chasmata monohydrated sulfates are detected in association with massive, light-toned material, forming steep slopes (Figure 9a). They are almost always identified along with nanophase ferric oxides along the ILD scarp, but they are observed also mixed with hematite and crystalline ferric minerals at lower elevations, at the base of the ILD, and on the canyon floor [*Murchie et al.*, 2009b] (Figure 6d).

On the contrary, polyhydrated sulfates dominate the mineralogy of the upper unit in Candor Mensa (Figures 5 and 7c). Polyhydrated sulfates are sometimes detected in the topmost part of the lower unit, but it is unclear at CRISM resolution whether they belong to the stratigraphy. These detections could actually reflect

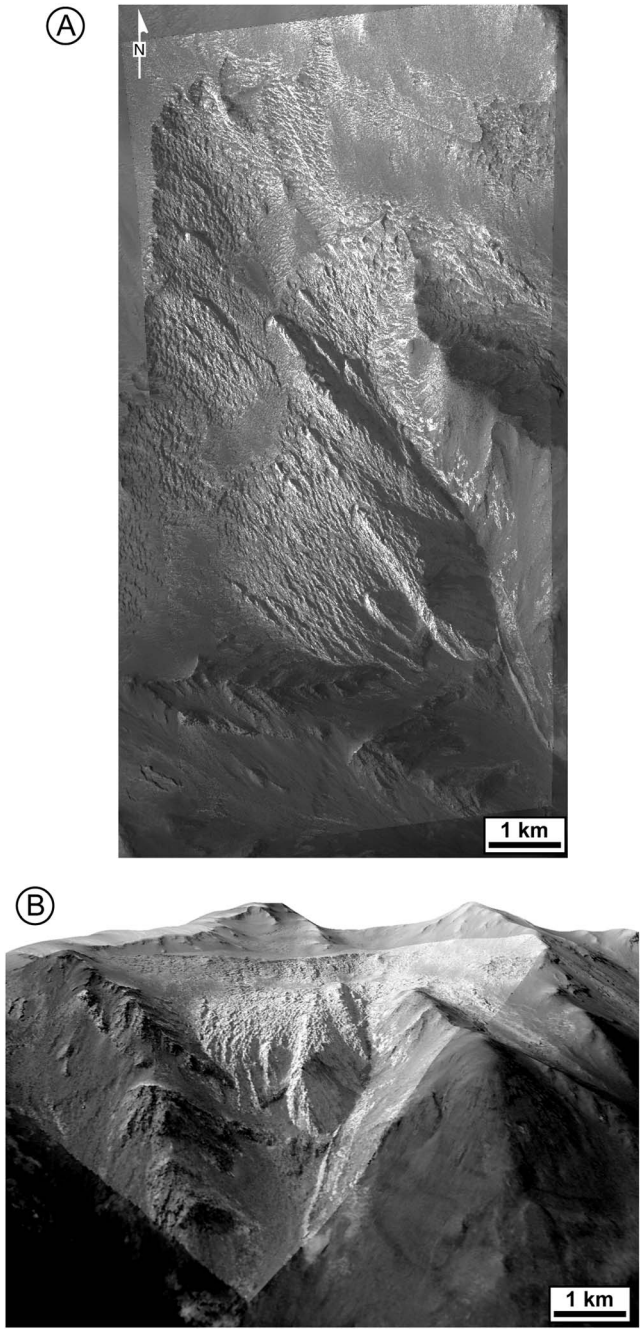

Figure 8. (a) Accumulation of light-toned material on northern wall between Candor and Ophir Chasmata (ESP_012018_1750). Location in Figure 1. (b) The main accumulation of light-toned material is located between two wall rock spurs and appears to exhibit nearly horizontal layering.

the composition of the bedrock and/or of a superficial coating. However, the morphological observations outlined below suggest that the latter hypothesis is less likely. Polyhydrated sulfates are also detected within loose material that seems eroded and carried away from the upper unit. Similar detections are made in the trough between the ILD northern flank and the wall of the canyon [*Mangold et al.*, 2008] (Figure 5). In the single CRISM observation in the northern trough that identifies both monohydrated and polyhydrated sulfates, no obvious geological contact can be identified in the corresponding HiRISE image. The monohydrated sulfate can visually be identified with lower unit geology, but whereas the outcrops of polyhydrated sulfates appear to be similar in composition to those of the upper unit, they do not have the same appearance of thin layers as observed at the top of Candor Mensa. Polyhydrated sulfates have not been detected at Baetis Mensa

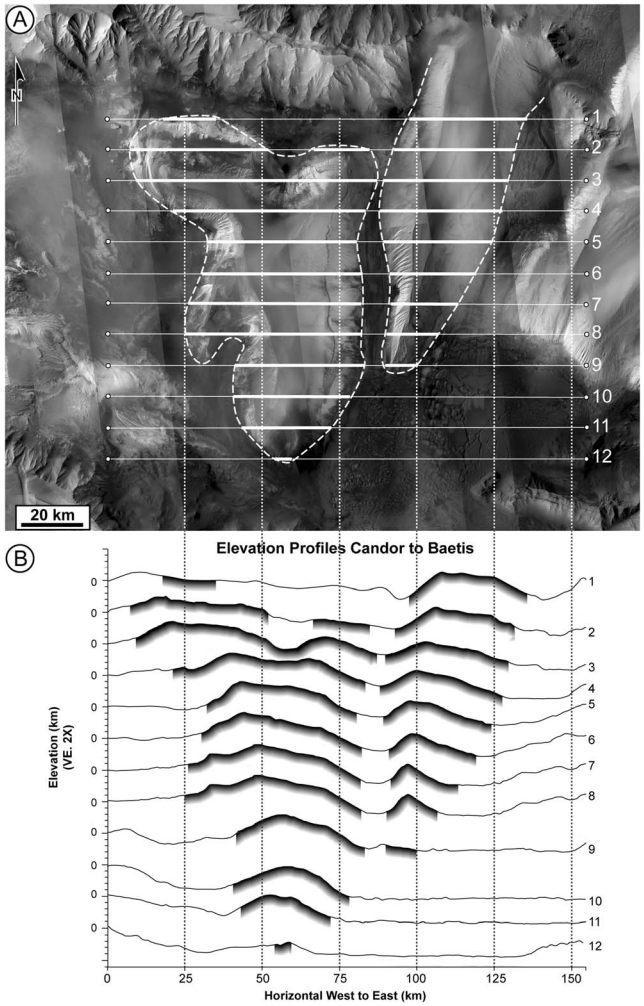

Figure 9. (a) Location of topographic profiles based on HRSC data across Candor and Baetis Mensae. Portions of the profile that correspond to the elevated mounds are shown with thicker white line. (b) Stack of topographic profiles, each offset by 5 km, with the 0 km elevation level shown for each profile. Sections of profiles corresponding to mound elevations (thick lines in Figure 9a) are shown as thick dark lines. Note the common eastward slope of both mensa surfaces 2 and 5 and the continuation of that slope for Candor Mensa in profiles 6–9.

so far, but they have been reported at high elevations in most of Valles Marineris ILDs [e.g., *Murchie et al*., 2009a; *Roach et al*., 2010].

The previously identified mixed phase is independent of the two units within Candor Mensa and is associated with allochthonous material that constitutes the lower part of the dark capping layer (Figures 5 and 7b). The top of the capping layer, which is made of dark material, does not bear such a signature. Indeed, the detection is limited to a few pixels on the edge of the capping layer outcrops, where the uppermost dark aeolian material seems removed and where higher albedo material is observed (Figures 6c and 7b). This bottom part of the capping layer has a lower albedo than the kieserite-rich lower unit that it often overlaps. Its orientation and pattern clearly allow us to connect this material to the capping layer and not to the underlying ILD unit (Figure 7b). The capping layer is also covering the upper unit, but the relative flatness of the upper unit and its polyhydrated sulfate-rich composition make it harder to identify the mixed phase by contrast.

5. Regional Context of Candor Mensa

Located immediately to the east of Candor Mensa is Baetis Mensa. To the east of Baetis Mensa is a large ILD mound on the western edge of East Candor Chasma. Separating these three ILDs are two narrow, deep, and straight channels. The overall geometry of these deposits and their locations already led Komatsu and his colleagues to suggest that it "would have been remarkable if they were not once part of a single deposit"

[*Komatsu et al*., 1993, p. 11108]. Hence, it is worthwhile to examine more recent data of the region around Candor Mensa. Determining the original extent of these deposits would allow for a better quantification of the amount of erosion they have undergone, which, in turn, enables a more accurate delineation of the geological history of the area.

Baetis Mensa overlaps the wall rock ridge forming the boundary between Ophir and Candor Chasmata. *Lucchitta* [2001] showed layered material in the wall separating Ophir Chasma from East Candor Chasma, whereas *Chojnacki and Hynek* [2008, Figures 7 and 8a] found sulfate-bearing light-toned material on the north side of the wall rock ridge between Ophir and West Candor Chasmata. HiRISE image PSP_005676_1750, located on the southern side of the wall between Ophir and West Candor Chasmata (Figure 8, location in Figure 1), shows outcrops of a thick accumulation of light-toned material, similar in appearance and composition to the lower unit material, on top of wall spurs at elevations of −200 m to −2800 m.

No layering is exposed on either side of the channel between Candor and Baetis Mensae, so no stratigraphy can be correlated. The western flank of Baetis Mensa exhibits more fluting than does the eastern flank of Candor Mensa, and topographic slopes are in the same general 15°–20° range (Figure 1c, slope map). A series of west-to-east topographic profiles across Candor and Baetis Mensae (Figure 9) indicates that the top of Candor Mensa is consistently above the top of Baetis Mensa and that the plateaus on top of both mensae adjacent to the channel slope to the east by approximately 6°. This direction is opposite to the general dip of the layering itself.

6. Discussion

6.1. Nature of Layering

Both the upper and lower units exhibit continuous layering with thicknesses on the scale of one to several meters. The existence of benches indicates a competency contrast between layers. Even though some larger benches appear to consist of several layers, no consistent finer internal layer structure can be identified. Layering that is thinner than the HiRISE image resolution of ~25cm might still be detected in shallow oblique sections, such as the tops of the benches of the lower unit, provided the layering displayed color and/or albedo contrasts.

Following previous suggestions [e.g., *Lucchitta*, 1990; *Chapman*, 2002; *Hynek et al*., 2003] that the deposits are the result of subaerially deposited pyroclastic material, we will suggest below that airborne dust or ash are attractive options for the source of sediments due to the wide lateral extent of the layers. Whereas proximal deposits of individual terrestrial supervolcano eruptions can be many meters thick, distal deposits produce layers on the order of centimeters to decimeters [e.g., *Matthews et al*., 2012]. Because there are no identified major volcanic centers nearby, the meter-scaled layers observed on Candor Mensa, especially those of the lower unit, are unlikely to represent single volcanic events.

6.2. Origin of the Sulfates

On Earth, sulfates are produced in a wide range of wet environmental conditions including shallow lakes and deep marine basins [e.g., *Cojan and Renard*, 1999; *Spencer and Hardie*, 1990; *Schreiber and Tabakh*, 2000], periglacial environments [e.g., *Bao et al*., 2000; *Wentworth et al*., 2005], hydrothermal systems [e.g., *Hannington and Scott*, 1988; *Swayze*, 1997], and even acidic rainfalls [*Brezonik et al*., 1980]. On Mars, their exact origin remains debated, although they do imply the presence of a water supply and a sulfur source at the time of their formation [*Gendrin et al*., 2005; *Bibring et al*., 2006]. Possible water sources include standing bodies of water (lakes), groundwater surges, and snow or ice melts. In the absence of any reported volcanic vents in or near Candor Chasma, it is reasonable to assume that the sulfur was present in the parent rocks or water. Atmospheric sulfur (or water) could have also contributed to the formation of sulfates, but then the alteration would be limited to the surface. As sulfates are detected over the entire ILD and do not seem to correspond to a surficial layer, and as they do not seem to show variation in absorption strengths with depth, we assume that they are present throughout the bulk of the ILDs and will not further consider the possibility of purely surficial alteration.

Our mineralogical observations alone do not allow us to determine the exact formation mechanism; all previously suggested models, such as the "snowmelt model" [*Kite et al*., 2013], "groundwater model" [*Andrews-Hanna et al*., 2007, 2010], and the lake hypothesis [*Quantin et al*., 2005] could represent possible settings. The snowmelt model considers the seasonal formation of sulfates by aqueous cementation of aeolian materials trapped into a snowmelt [*Kite et al*., 2013]. This model could explain the limited distribution of sulfates on Mars to the few areas

of seasonal snowmelt (Valles Marineris and Terra Meridiani). This model would result in a top-down weathering and has the advantage of working well under the expected cold and dry conditions of the Hesperian. The alternative groundwater model [*Andrews-Hanna et al*., 2007, 2010] considers the formation of sulfates due to a rising water table, followed by massive and repeated evaporation [*Arvidson et al*., 2006]. This model has been favored in the Terra Meridiani area as it has been identified as a region of groundwater upwellings [*Andrews-Hanna et al*., 2007] and is supported by the Opportunity rover's in situ observations of lithified sands [*Grotzinger et al*., 2005]. The level to which the water table has risen would then determine which thickness of the ILD has been weathered from bottom to top. Previous work suggests that this model is also viable for Candor Chasma; considering repeated groundwater upwellings and a moderate evaporation rate, an ~5 km thick evaporate deposit could be formed in about 400 My [*Murchie et al*., 2009b]. A last possibility is the formation of sulfate-rich deposits by evaporation in a lake. This mechanism has rarely been favored, given the expected cold and dry conditions during the Hesperian that would make a standing body of water improbable, but is a reasonable formation mechanism for sulfates. It remains unlikely, given the timing of the sulfate formation (to be discussed below) and the thickness of the ILD, that Candor Mensa could be made completely of evaporites. However, evaporites could have precipitated as a cement between existing sediments, or the ILD could have formed from the acidic weathering of preexisting S-bearing sediments.

6.3. Sulfate Hydration State and Stratigraphy

Our observations show two distinct sulfate-bearing units of different hydration state: the lower unit, dominated by Mg-monohydrated sulfate (kieserite) signatures, and the upper unit, dominated by (likely Mg or Fe-rich) polyhydrated sulfate signatures. The facts that the two units also differ in other aspects (albedo, layer thicknesses, slope…) and that the boundary between sulfate types coincides with the unit stratigraphic boundary suggest that a difference in composition or environment is the most likely explanation. Although we could not conclude that the polyhydrated sulfates found at low elevations in the northern trough were part of the stratigraphy in Candor Chasma, their occurrence stratigraphically beneath monohydrated sulfate-rich outcrops in other chasmata (e.g., Capri Chasma [*Flahaut et al*., 2010b]) also argues against late dehydration/rehydration mechanism or burial diagenesis as a possible explanation for the observed difference in hydration state in most of Valles Marineris ILDs, as previously tested by *Roach et al*. [2009]. Possible explanations for the difference in composition between the lower unit (kieserite-bearing material) and upper unit (polyhydrated sulfate-bearing material) may be the quantity of water present at the time (a higher water/rock ratio is required to form polyhydrated sulfates) of sulfate formation, the composition of the protolith (Mg-rich for the formation of kieserite in the lower unit, potentially Fe-rich for the upper unit?), the environmental conditions (temperature and pH), and/or the chemistry of water. We will argue below that the upper unit is not likely to have formed at a higher water/rock ratio or different temperature range due to its timing of formation. Therefore, we suggest that the difference in hydration between the lower and upper units is more likely related to a different parent material or water chemistry/source. These observations are consistent with layering measurements and morphological observations which also support a different origin and timing for both units.

6.4. Sulfate Timing

The sulfate mineralogy alone does not provide any data regarding the timing of their formation. If sulfates formed during a single event following the deposition of the upper unit, then differences in protolith composition of the two units would be required to form both polyhydrated and monohydrated sulfates in the close proximity that is documented near the top of Candor Mensa. If the source of the sediment for both units is the same, then different water composition, source and/or environmental conditions are necessary to account for the difference in hydration states, suggesting that the formation of the sulfates took place during at least two different aqueous episodes, discussed in more detail below. Given that aeolian sediments appear to be the most likely source of material for both units (sections 6.1 and 7) and assuming they have similar compositions, we will favor a multiple stage of sulfate formation in the proposed geologic history hereafter.

6.5. The Original Extent of Candor Mensa

It is also important to consider the scale over which formation mechanisms have been active. *Komatsu et al*. [1993] suggested that a single deposit originally extended to the wall between Ophir and Candor Chasmata

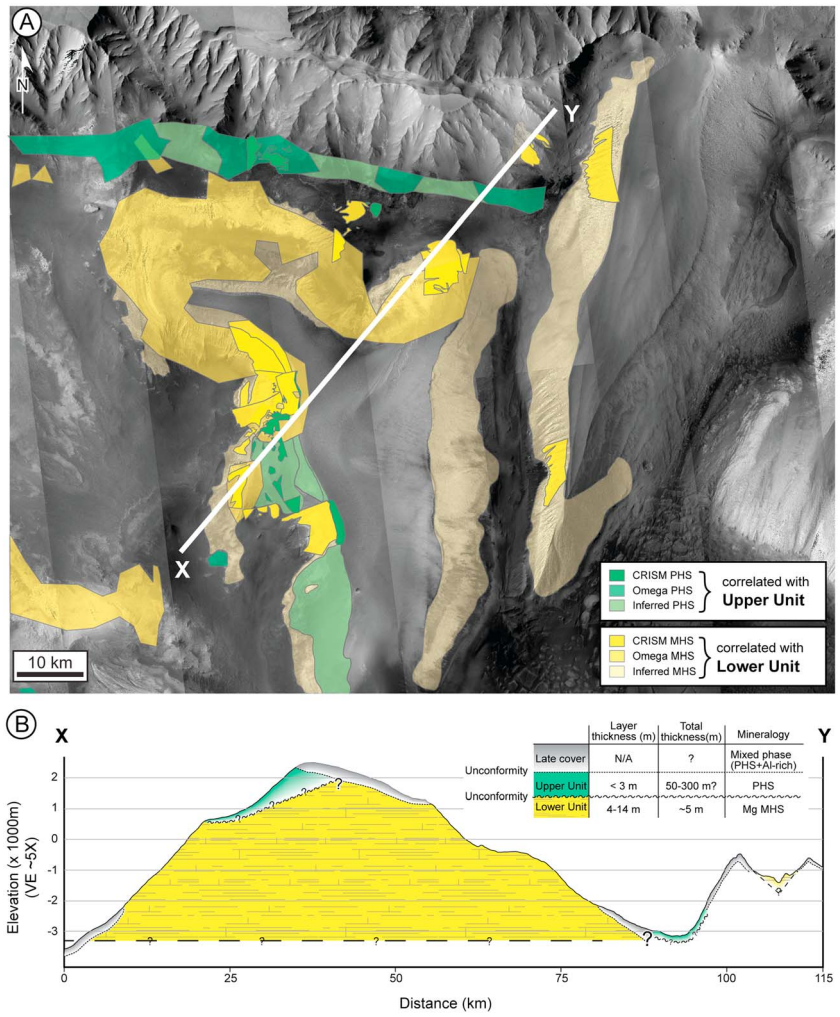

Figure 10. (a) Simplified geological map of outcrops of units based on CRISM and OMEGA data, extended by visual examination of CTX images. Where CRISM and OMEGA data differ (see Figure 7), e.g., along line XY, the newer CRISM data are favored because this also agrees with visible geology as discussed in the text. (b) Cross section (vertical exaggeration 5×). Contacts of units within mound are unknown. The table summarizes the main properties of each unit.

and included Candor and Baetis Mensae, as well as the deposit east of Baetis Mensa. The identification of outcrops bearing monohydrated sulfates on the eastern flank of Baetis Mensa and on the northern wall between Ophir and Candor Chasmata [e.g., *Chojnacki and Hynek*, 2008], as well as the topographic similarities between Candor and Baetis Mensae, strengthens that interpretation.

Hence, we concur with the suggestion of *Komatsu et al.* [1993] that Baetis Mensa and quite possibly the deposit east of Baetis Mensa were part of proto-Candor Mensa which most likely extended to the northern wall rock ridge. There is no obvious way similarly to constrain the original western extent of Candor Mensa. We suggest that the original, or proto-Candor Mensa, deposit measured a minimum of 150 km north to south and 130 km east to west, covering 19,500 km^2. If its current maximum height, chosen as the preerosion height of 8 km extended over its entire extent, it would comprise a volume of 156,000 km^3. This estimate must be considered conservative. One complicating factor is that Baetis Mensa actually covers the easternmost portion of the northern wall rock ridge where its elevation drops significantly (Figure 1c) and thus effectively continues into Ophir Chasma. Because we did not include Ophir Chasma in our present study and because the more elevated western portion of the wall rock ridge would provide an effective northern limit for the bulk of Candor Mensa, we use the provided minimum estimate. This proto-Candor Mensa deposit must have experienced one or most likely several massive erosion events leading to isolated mounds, as discussed below.

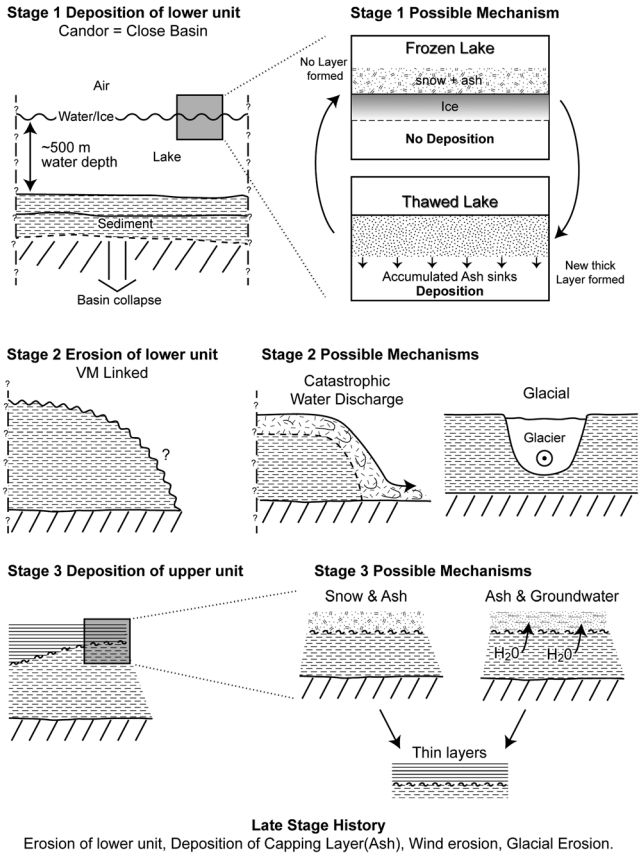

Figure 11. Three-stage model of geological history of Candor Mensa. See text for discussion.

7. A Model for the Geological History of Candor Mensa

The observations presented above cover the available mineralogical, stratigraphic, and topographic data. The data allow for the construction of a simplified map and cross section of the area (Figure 10). For the map we correlate outcrops visually identified as lower unit with other outcrops of monohydrated sulfates. As discussed above, we tentatively assign a series of polyhydrated sulfate outcrops within the northern trough to the upper unit. As indicated in the cross section, the outcrop of lower unit within the northern wall is topographically above these polyhydrated sulfate outcrops but well within the elevation range of the lower unit within the main body of Candor Mensa. The nature of the contact between units is indicated, but the extent of the upper unit is unknown. Pertinent facts about the two units are summarized in the table in Figure 10.

The data provide enough information to propose a geological history of this area and to propose models for the deposition and erosion of Candor Mensa. That history can be divided into three major stages which have been illustrated in Figure 11 and are discussed in detail below.

7.1. Stage 1—Deposition of the Lower Unit

The lower unit consists of a minimum measured stratigraphic height of 3 km but can visually be traced over approximately 5 km of elevation, which given the low layer dips corresponds to about 5 km of stratigraphy. Hence, it comprises the bulk of the volume of Candor Mensa. It consists of regionally extensive parallel layers with relatively consistent thickness and devoid of any internal structures. No unconformities, evidence of channels, or systematic thickness variations are found within the approximately 5 km of stratigraphy.

Effectively this rules out many more localized sources such as nearby volcanic sources, river systems, or alluvial or other fans or the possibility that significant volumes of ILD could be derived by slumping of wall rock material. The size and uniformity of Candor Mensa also does not make it a good candidate for a spring deposit, but rather suggests a distal source with a wide dispersal mechanism. More constraints are provided by the lower unit

mineralogy, which is dominated by kieserite. The presence of sulfates implies that a water supply was present during or after the formation of the lower unit. Given the thickness of the lower unit and the homogenous signatures at CRISM scale, precipitation from acidic brines or weathering of sulfur-bearing rocks in a shallow lake or during repeated groundwater upwelling appear to be the most likely mechanisms.

The evaporative groundwater discharge model used by *Murchie et al*. [2009b] requires on the order of 400 My to produce a 5 km high ILD mound of evaporite-cemented eolian sediment within Candor Chasma. However, recent geophysical modeling [*Andrews-Hanna*, 2012b] suggests that the time to collapse of the basin may only be on the order of 10–100 My. Another longstanding hypothesis, namely that ILDs were formed in a lacustrine setting [e.g., *Nedell et al*., 1987; *Quantin et al*., 2005], has recently been extensively reviewed by *Lucchitta* [2010, and references therein]. *Warner et al*. [2013] provided convincing evidence that basins in eastern Valles Marineris were filled with water, which spilled over the chasm walls. It seems unlikely that some isolated basins within Valles Marineris were filled with water while others provided an intermittently wet eolian setting.

Hence, we propose that the deposition of the lower unit proceeded in an enclosed basin, which following the suggestion of *Warner et al*. [2013] was filled with water. At its minimum, its regional extent included both Candor and Baetis Mensae with the northern wall rock ridge forming the northern limit for Candor Mensa, though Baetis Mensa likely extended into Ophir Chasma. *Lucchitta et al.* [1994] originally envisaged basins as lakes with water depth of several kilometers which would require rapid collapse and abundant water but limited sediment supply. A shallower lake may be expected if deposition kept up with subsidence during basin collapse [*Fueten et al*., 2008]. The model by *Andrews-Hanna* [2012b] requires that basin subsidence must be driven by sediment influx to remain in isostatic equilibrium. This limits the water depth to a maximum of approximately 500 m [*Andrews-Hanna*, 2012b] if water filled the basin to the approximate level of the plateau as suggested by *Warner et al*. [2013]. Given the stratigraphic consistency of the unit, we suggest that the water depth within the lake was no more than several hundred meters and that the collapse occurred as multiple events. We found no geological features that could be correlated with this collapse; it may be that extensively disrupted sediments in regions along boundary faults eroded preferentially. The water depth, along with the layering continuity, suggests that the lake did not experience repeated extensive dry periods and that the majority of the ILD was deposited in a lacustrine setting. Any physical or mineralogical evidence of potential dry periods was likely eliminated during the next flood stage.

One aspect that requires addressing is what mechanism would produce the documented meter-scale layering in a lacustrine setting, if a single layer cannot correspond to an individual volcanic event, as argued above. To produce the 3 km of stratigraphic thickness over which the layer thickness was measured to be between 4 and 12 m, approximately 400 to 500 layer-producing events would have been required. Ignoring the portion of the ILD for which we have no layer thicknesses but using an estimate of 500 layers and a basin collapse time of 10–100 My [*Andrews-Hanna*, 2012b] suggests that each layer corresponds to an event of 20,000 to 200,000 years. This estimated deposition interval is comparable to the current periodicity of the obliquity of Mars of approximately 120,000 years [*Laskar et al*., 2005]. Unfortunately, it is not possible to accurately calculate the obliquity parameters for distant geological time periods [*Laskar et al*., 2005].

The obliquity of Mars has a strong effect on its climate. Modeling of Amazonian climate [*Madeleine et al*., 2009] suggests that ice accumulation within Valles Marineris could have led to the formation thick regional ice sheets, and *Gourronc et al*. [2014] argued that the landforms within the chasms of Valles Marineris were extensively glaciated during Late Noachian to Early Hesperian times. During glacial periods a lake would have been frozen and hence we suggest that the lake alternated between frozen and liquid states, possibly corresponding to obliquity cycles.

Terrestrial perennially frozen Antarctic lakes have been considered as analogues for the Martian setting. *Nedell et al*. [1987] and *Squyres et al*. [1991] studied Lake Hoare within the Dry Valleys of Antarctica. It is surrounded by a moat of open water annually with a porous ice cover that would channel sediment into ice fractures and lead to a very inhomogenous mode of sediment deposition [*Squyres et al*., 1991]. By contrast, the 240 km long Lake Vostok is covered by a 3.7 to 4.1 km thick ice sheet that may have been stable for the last 20 million years. The ice sheet travels across the lake, where melting and freezing at its base controls the water depth and sediment influx [e.g., *Siegert et al*., 2001]. Neither one of these examples is likely a perfect analogue for a frozen lake in Candor Chasma, but we do not envisage annual freeze-thaw cycles.

We suggest that ash, dust, and snow would accumulate on top of the frozen ice surface which remained frozen for extended periods of time. Minor amounts of larger fragments (e.g., chunks of wall rock) may also have been transported onto the frozen lake, but no evidence of such clasts was found within the ILD. Very little or no sediment deposition in the basin would take place while the surface was frozen. Deposition of accumulated sediment on the basin floor would primarily take place during the melting episodes. The mechanism by which this breakup was able to deposit homogenous thick layers is uncertain, though it clearly depends on the properties of the ice/sediment mixture as well as on the nature of the melt event. The melting itself may have been triggered by external warming at the end of a period of obliquity or by internal heat flow as an overlying cover would have served as a thermal insulator. *Zegers et al*. [2010] has suggested that buried ice sheets can melt through regular crustal heat flux when buried by 1–2 km of sediment. But unless the heat flux under Valles Marineris is several orders of magnitude higher than the heat flux assumed by *Zegers et al*. [2010], the observed 4–12 m thick blanketing layers would eliminate this as a viable mechanism here.

In summary, we suggest that the lower unit sediment was initially deposited on the surface of a frozen lake, with deposition to the basin floor occurring when the lake melts during warmer periods. The 4–12 m thick layering of the lower unit may thus be linked to obliquity cycles.

7.2. Stage 2—Erosion of the Lower Unit

The contact between the upper and lower units is a disconformity that cuts several kilometers into the layering of the lower unit in places. Since we suggest that originally Candor Mensa extended to the northern wall and tentatively correlate the polyhydrated-sulfate-containing material within the northern trough to the upper unit material, the northern trough must have formed prior to the deposition of the upper unit. It is not possible to similarly constrain the erosion responsible for carving the channel between Candor and Baetis Mensae. *Fueten et al*. [2008] also argued for a significant erosion event southwest of Candor Mensa which removed much of an approximately 750–800 m thick regionally extensive ILD unit. Hence, large volumes of ILD material were mobilized during at least one and possibly several erosion events. At least some of that erosion has to predate the deposition of the later, Hesperian-age upper ILD unit. This relatively short time frame makes it unlikely that erosion by wind was a candidate. Other mechanisms are capable of removing large volumes in relatively short geological time periods.

Komatsu et al. [1993] suggested that a catastrophic water release over a short time is a possible mechanism for the removal of ILD material. *Komatsu et al*. [1993, p. 11,116] estimated the volume removed to be on the order of 15,000 km^3 and possibly an order of magnitude more. A volume calculation using the HRSC DEM indicates that the gap between Candor Mensa and the northern wall and the channel between Candor and Baetis Mensa account for approximately 25,420 km^3.

More recently, *Kite et al*. [2013] suggested that periodic snowmelt may also be an erosive mechanism. However, it is questionable whether it could have been responsible for the large-scale erosion illustrated here.

Glacial erosion is another possible mechanism, especially during times of high obliquity. In addition to climate modeling [*Madeleine et al*., 2009], evidence for possible glaciers inside the Valles Marineris has previously been discussed [e.g., *Chapman et al*., 2005; *Mège and Bourgeois*, 2011; *Gourronc et al*., 2014]. *Fueten et al*. [2011b] suggested that two smaller hollows within an ILD in Coprates Chasma are the result of glacial scours. The channel between Candor and Baetis Mensae is comparable to the dimensions of some of Earth's glaciers (e.g., Nimrod glacier in Antarctica is 200 km long and 18 km wide [*Swithinbank*, 1988]) and has been proposed to be a channel for ice flow [see *Gourronc et al*., 2014, Figure 13].

Erosion by either large-scale water release or glaciers would have mobilized large volumes of material which had to be deposited in another location. If the basin needs to be filled by sediment in order for it to subside [*Andrews-Hanna*, 2012b], little room is left for large volumes of erosional material within a closed chasm. To create space and a pathway for remobilized ILD material, the extent of the basin therefore needed to be modified. The two-stage model for the evolution of Valles Marineris [*Schultz*, 1998] incorporates such modification. The model proposes that the initially isolated basins, such as Candor and Ophir Chasmata, were linked into the current system during a significant tectonic event. This linking of Candor Chasma with Melas and presumably Coprates and Ius would have provided the room and passageways for the removal of the material. Hence, we suggest that the period of erosion coincides with the tectonic activity that linked the isolated basins and produced the current geometry of Valles Marineris. Any catastrophic water release was

likely restricted to the initial opening of the basin. The primary source of this water would be the up-to-500 m of water within the closed basin plus pore water liberated from within the ILD. The erosive force would clearly depend upon the nature of the linking of the isolated chasmata. By contrast, glacial erosion could take place during multiple episodes, perhaps associated with obliquity cycles. The common eastward slope of the top surface of both Candor and Baetis Mensae (Figure 5b) may be the result of early erosion when both were part of a single larger ILD. By contrast, the formation of the channel separating them dates to a later episode.

We have no constraints on the duration of this erosional period. Given the differences between the upper and lower units, the tectonism permanently changed the deposition environment for ILDs. We suggest that the possibility of standing water at significant elevations after Valles Marineris had attained its current geometry is unlikely. *Lucchitta* [2010] discussed late shallow lakes within Valles Marineris (VM) at low elevations. Such water may have been present within the troughs but not near the top of Candor Mensa, at the site of the deposition of the upper unit.

7.3. Stage 3—Deposition of Upper Unit

The upper unit consists of thinner layers than in the lower unit and is an overall thinner stratigraphic package (estimated to be 50–300 m thick), disconformably deposited on top of the lower unit following a period of erosion. It can be identified only over a smaller regional extent, though it is uncertain whether this is due to later erosion or limited original deposition.

Layers of the upper unit are parallel, with no internal structures and no observed unconformities or channels. This unit is unlikely to be of aeolian origin since tabular crossbeds would be larger than the thin beds observed. We argued above that the linking of VM would make the presence of standing water at the time of deposition of the upper unit problematic, especially at elevations near the top of Candor Mensa. We suggest that aerially deposited dust or ash are the most likely sources of material for this unit.

The upper unit contains polyhydrated sulfates, spectrally identical to polyhydrated sulfates identified at lower elevation between the wall rock ridge and Candor Mensa (Figure 5). Polyhydrated sulfates at low elevations have previously been assigned tentatively to low stratigraphic levels [e.g., *Flahaut et al*., 2010a, Figure 5; *Mangold et al*., 2008, Figure 18; *Chojnacki and Hynek*, 2008, Figure 6]. However, there is no stratigraphic evidence that they belong to another, lowermost unit in Candor Chasma. We have demonstrated that the polyhydrated sulfate material on top of Candor Mensa has been disconformably deposited following a period of erosion. Hence, the geologically simplest explanation for this region is that the polyhydrated sulfate material at low elevations is stratigraphically identical to the polyhydrated material on top of Candor Mensa and was also deposited disconformably, following the same period of erosion. Given the uncertainties discussed above, this interpretation is tentative until clear geological boundary relationships can be established. Since the formation of polyhydrated sulfates requires interaction with water, two separate scenarios are suggested.

Kite et al. [2013] proposed a snowmelt hypothesis, in which the melting snow can provide the water necessary for the cementation of sedimentary rocks. Hence, we suggest that periodic melting of an accumulated mixture of snow, ash, and dust on top of Candor Mensa would produce a thin layer of the upper unit by cementing the solids during a melt episode. The melting of the mixture snow and solids would concentrate the solids which could then be cemented into a layer. This mechanism would work well on top of the exposed Candor Mensa.

Another, perhaps complementary, mechanism involves the action of groundwater, as has been suggested for this region by *Mangold et al*. [2008], though the elevated and isolated location near the top of Candor Mensa is not an ideal environment for groundwater flow.

The thinner layers of the upper unit and the possible thinning trend through this unit may be the result of the formation mechanism. The melting of a surface layer of snow in particular would require less warming than the melting of a thick ice sheet covering a lake. Snowmelt or periodic groundwater infusion may thus occur on a shorter timescale than the large-scale melting envisaged for the lower unit. Thinner layers may also reflect a decrease in sediment supply. Depending on the duration of the period of erosion, the available volume of volcanic ash within a given time period may well be less for the upper unit than for the lower unit. This may point to a reduction of volcanic activity during this deposition period.

7.4. Late-Stage History

Both ILD units are partly covered by a dark, smooth, unconformable layer referred to as the capping layer, which also covers much of the northern wall between Candor and Ophir Chasmata. The wide distribution of

observed locations indicates that its deposition postdates the erosion of the entire ILD. However, given the uncertainties of the upper unit's original extent or thickness, no details of this erosion can be given at this stage. Since this late-stage history likely spanned billions of years and features attributed to wind erosion or impacts are prominent, wind erosion was a major erosive mechanism. However, the existence of late glaciers or snowmelt episodes throughout the Amazonian cannot be ruled out, especially since the capping layer shows evidence of hydration.

This capping layer has been commonly reported as a thin late aeolian cover on Valles Marineris ILDs and generally shows a neutral or mafic-rich mineralogical signature [*Mangold et al*., 2008]. However, we noticed for the first time that parts of this capping layer in Candor Chasma, especially at the layer's base, show signatures of hydrated minerals (referred to as a mixed phase in this paper) and particularly Al-rich phases and sulfates. Although there is no clear consensus on the origin or age of the layer, the hydration of its basal part suggests either (1) a change in the source material, likely aeolian in origin, that was made of originally hydrated material or (2) partial alteration during or after deposition. In this last case, the presence of Al-rich material could evidence surface processes such as pedogenesis or surface leaching but could also indicate that the parent material of this unit was more felsic in composition than the ILD parent material. In all cases it implies that local aqueous processes and hydrated mineral formation still occurred locally after the formation and erosion of Valles Marineris in the Amazonian. Evidence for pedogenesis on the plateaus surrounding Valles Marineris during the Hesperian has been documented by *Le Deit et al*. [2012].

8. Conclusions

We have examined the geology and mineralogy of Candor Mensa and its immediate surroundings. The geology of this up-to-8 km high ILD can be divided into two major units. The lower unit, which accounts for at least 5 km of strata, is characterized by 4 to 12 m thick, uniform, parallel layering. This layering is devoid of internal sedimentary features at HiRISE scale and associated with monohydrated sulfates. The upper unit is characterized by thinner, 1 to 4 m thick layering, and near the top of Candor Mensa it is exclusively associated with polyhydrated sulfates. The contact between the two units is clearly unconformable and indicates that the upper unit was emplaced following a significant period of erosion of the lower unit. Further evidence suggests that Candor and Baetis Mensae may have originally been one single deposit that also extended to the northern wall between Candor and Ophir Chasmata.

We propose a geological history in which the lower unit was deposited in isolated water-filled basins (lakes), prior to Valles Marineris achieving its current geometry. These lakes would have been frozen during periods of high obliquity. The thicker layers of the lower unit initially accumulated as ash or dust on top of the frozen lake surface, subsequently depositing as a single sedimentary layer during the thawing of that lake. The freeze-thaw cycle of the lakes and therefore the layering may have been linked to obliquity cycles.

Faulting and subsidence of the regions surrounding the ILDs during the formation of Valles Marineris caused linking of individual basins to form the current geometry, allowing the removal of the basin water. Catastrophic release of water during this stage, along with boundary faulting and possible glacial action, caused erosion of the lower unit body.

Eventually, the erosion processes ceased and deposition of ash or dust on an exposed surface continued, forming the much thinner layers of the upper unit. Cementation of these layers is postulated to be the result of either groundwater or the snowmelt mechanism proposed by *Kite et al*. [2013], as standing water at high elevations would no longer be possible at this stage.

The ultimate source of sediment for both units is thought to be airborne dust or ash. Since the environmental conditions for the deposition of the two units differ considerably, we suggest that the formation of the two types of sulfates is also linked to these differences in environment. Future work will be aimed to determine if previously documented differences in sulfate mineralogy [e.g., *Flahaut et al*., 2010a] can also be linked to differences in sedimentary environment.

The late-stage history of this area is dominated by the deposition of a late capping layer and extensive wind and possibly glacial erosion. The capping layer shows signatures of hydrated minerals providing evidence that hydrated mineral formation was possible after the formation and erosion of Valles Marineris in the Amazonian.

Acknowledgments

We thank the HRSC experiment teams at DLR Berlin and Freie Universitaet Berlin and the Mars Express project teams at ESTEC and ESOC for their successful planning and acquisition of data, as well as for making the processed data available to the HRSC team. We also want to thank the CTX, HiRISE, and CRISM teams for making their data available. This project was partially funded by an NSERC discovery grant to F. Fueten. Pangaea Scientific thanks P. Budkewitsch and Canada Centre for Remote Sensing for support of Orion under contract NRCan-01-0102. E. Hauber was partly funded by the Helmholtz Alliance "Planetary Evolution and Life". J. Flahaut is funded by a Netherlands Organisation for scientific research (N.W.O) VENI Innovational Research grant. We thank M. Lozon for preparing the illustrations. We also thank the International Space Science Institute (ISSI) for their support by providing the authors with an opportunity to discuss the topic and the team members for their collaboration. This manuscript was significantly improved by the thorough reviews of Matthew Chojnacki and Chris Okubo and by constructive comments by the Editor, David Baratoux.

References

Andrews-Hanna, J. C. (2012a), The formation of Valles Marineris: 1. Tectonic architecture and the relative roles of extension and subsidence, *J. Geophys. Res.*, *117*, E03006, doi:10.1029/2011JE003953.

Andrews-Hanna, J. C. (2012b), The formation of Valles Marineris: 3. Trough formation through super-isostasy, stress, sedimentation, and subsidence, *J. Geophys. Res.*, *117*, E06002, doi:10.1029/2012JE004059.

Andrews-Hanna, J. C., R. J. Phillips, and M. T. Zuber (2007), Meridiani Planum and the global hydrology of Mars, *Nature*, *446*(7132), 163–166.

Andrews-Hanna, J. C., M. T. Zuber, R. E. Arvidson, and S. M. Wiseman (2010), Early Mars hydrology: Meridiani playa deposits and the sedimentary record of Arabia Terra, *J. Geophys. Res.*, *115*, E06002, doi:10.1029/2009JE003485.

Arvidson, R. E., et al. (2006), Nature and origin of the hematite-bearing plains of Terra Meridiani based on analyses of orbital and Mars Exploration rover data sets, *J. Geophys. Res.*, *111*, E12S08, doi:10.1029/2006JE002728.

Bao, H., D. A. Campbell, J. G. Bockheim, and M. H. Thiemens (2000), Origins of sulphate in Antarctic dry-valley soils as deduced from anomalous ^{17}O compositions, *Nature*, *407*, 499–502.

Bibring, J. P., A. Soufflot, and J. Mustard (2004), OMEGA: Observatoire pour la Mineralogie, l'Eau, les Glaces, et l'Activite, *ESA Spec. Publ.*, *1240*, 37–49.

Bibring, J.-P., et al. (2005), Mars surface diversity as revealed by the OMEGA/Mars Express observations, *Science*, *307*, 1576–1581, doi:10.1126/science.1108806.

Bibring, J.-P., et al. (2006), Global mineralogical and aqueous Mars history derived from OMEGA/Mars Express data, *Science*, *312*, 400–404, doi:10.1126/science.1122659.

Bibring, J.-P., et al. (2007), Coupled ferric oxides and sulfates on the Martian surface, *Science*, *317*, 1206–1210, doi:10.1126/science.1144174.

Bishop, J. L., et al. (2009), Mineralogy of Juventae Chasma: Sulfates in the light-toned mounds, mafic minerals in the bedrock, and hydrated silica and hydroxylated ferric sulfate on the plateau, *J. Geophys. Res.*, *114*, E00D09, doi:10.1029/2009JE003352.

Brezonik, P., E. S. Edgerton, and C. D. Hendry (1980), Acid precipitation and sulfate deposition in Florida, *Science*, *208*, 1027–1029, doi:10.1126/science.208.4447.1027.

Broxton, M. J., and L. J. Edwards (2008), The Ames Stereo Pipeline: Automated 3D surface reconstruction from orbital imagery, Lunar Planet. Sci., XXXIX, Abstract #2419.

Carr, M. H., and J. W. Head (2010), Geologic history of Mars, *Earth Planet. Sci. Lett.*, *294*, 185–203, doi:10.1016/j.epsl.2009.06.042.

Catling, D. C., S. E. Wood, C. Leovy, D. R. Montgomery, H. M. Greenberg, C. R. Glein, and J. M. Moore (2006), Light-toned layered deposits in Juventae Chasma, Mars, *Icarus*, *181*, 26–51, doi:10.1016/j.icarus.2005.10.020.

Chapman, M. G. (2002), Layered, massive, and thin sediments on Mars: Possible Late Noachian to Late Amazonian tephra?, in *Volcano-Ice Interactions on Earth and Mars*, vol. 202, edited by J. L. Smellie and M. G. Chapman, pp. 273–203, Geol. Soc. Spec. Publ., London, doi:10.1144/GSL.SP.2002.202.01.14.

Chapman, M. G., and K. L. Tanaka (2001), Interior trough deposits on Mars: Subice volcanoes?, *J. Geophys. Res.*, *106*(E5), 10,087–10,100.

Chapman, M. G., L. A. Soderblom, and G. Cushing (2005), Evidence of very young glacial processes in central Candor Chasma, Mars, Lunar Planet. Sci., XXXVI, Abstract 1850.

Chojnacki, M., and B. M. Hynek (2008), Geological context of water-altered minerals in Valles Marineris, Mars, *J. Geophys. Res.*, *113*, E12005, doi:10.1029/2007JE003070.

Christensen, P. R., R. V. Morris, M. D. Lane, J. L. Bandfield, and M. C. Malin (2001), Global mapping of Martian hematite mineral deposits: Remnants of water-driven processes on early Mars, *J. Geophys. Res.*, *106*(E10), 23,873–23,885, doi:10.1029/2000JE001415.

Clark, R. N., T. V. V. King, and N. S. Gorelick (1987), Automatic continuum analysis of reflectance spectra, in *Proceedings of the Third Airborne Imaging Spectrometer Data Analysis Workshop*, vol. 87-30, pp. 138–142, JPL Publication, Pasadena, Calif.

Clark, R. N., T. V. King, M. Klejwa, G. A. Swayze, and N. Vergo (1990), High resolution reflectance spectroscopy of minerals, *J. Geophys. Res.*, *95*(B8), 12,653–12,680.

Cloutis, E. A., et al. (2006), Detection and discrimination of sulfate minerals using reflectance spectroscopy, *Icarus*, *184*, 121–157.

Cojan, I., and M. Renard (1999), *Sédimentologie*, Masson ed., pp. 418, Coll. Enseignement des Sciences de la Terre, Paris.

Dohm, J. M., and K. L. Tanaka (1999), Geology of the Thaumasia region, Mars: Plateau development, valley origins, and magmatic evolution, *Planet. Space Sci.*, *47*, 411–431.

Flahaut, J., C. Quantin, P. Allemand, P. Thomas, and L. Le Deit (2010a), Identification, distribution and possible origins of sulfates in Capri Chasma (Mars), inferred from CRISM data, *J. Geophys. Res.*, *115*, E11007, doi:10.1029/2009JE003566.

Flahaut, J., C. Quantin, P. Allemand, and P. Thomas (2010b), Morphology and geology of the ILD of Capri/Eos Chasma (Mars) from visible and infrared data, *Icarus*, *207*, 175–185, doi:10.1016/j.icarus.2009.11.019.

Frey, H. (1979), Martian canyons and African rifts: Structural comparisons and implications, *Icarus*, *37*, 142–155, doi:10.1016/0019-1035(79)90122-2.

Fueten, F., R. Stesky, P. MacKinnon, E. Hauber, T. Zegers, K. Gwinner, F. Scholten, and G. Neukum (2008), Stratigraphy and structure of interior layered deposits in west Candor Chasma, Mars, from High Resolution Stereo Camera (HRSC) stereo imagery and derived elevations, *J. Geophys. Res.*, *113*, E10008, doi:10.1029/2007JE003053.

Fueten F., R. Harvey, R. Stesky, E. Hauber, and A. Rossi (2011a), Layer thickness determination of interior layered deposits, with particular emphasis on Candor Mensa, Mars, Lunar Planet. Sci. XLII, Abstract #1255.

Fueten, F., J. Flahaut, L. Le Deit, E. Hauber, and R. M. Stesky (2011b), Interior layered deposits within an ancestral basin in southern Coprates Chasma, Valles Marineris, Mars, *J. Geophys. Res.*, *116*, E02003, doi:10.1029/2010JE003695.

Gendrin, A., et al. (2005), Sulfates in Martian layered terrains: The OMEGA/Mars Express view, *Science*, *307*, 1587–1591.

Golombek, M. P., and R. J. Phillips (2010), Mars tectonics, in *Planetary Tectonics*, vol. 11, edited by T. R. Watters and R. A. Schultz, pp. 183–232, Cambridge Univ. Press, New York.

Gourronc, M., et al. (2014), One million cubic kilometers of fossil ice in Valles Marineris: Relicts of a 3.5 Gy old glacial landsystem along the Martian equator, *Geomorphology*, *204*, 235–255, doi:10.1016/j.geomorph.2013.08.009.

Grotzinger, J. P., et al. (2005), Stratigraphy and sedimentology of a dry to wet eolian depositional system, Burns formation, Meridiani Planum, Mars, *Earth Planet. Sci. Lett.*, *240*(1), 11–72, doi:10.1016/j.epsl.2005.09.039.

Hannington, M. D., and S. D. Scott (1988), Mineralogy and geochemistry of a hydrothermal silica-sulfide-sulfate spire in the caldera of Axial Seamount, Juan De Fuca Ridge, *Can. Mineral.*, *26*, 603–625.

Head, J. W., R. Greeley, M. P. Golombek, W. K. Hartmann, E. Hauber, R. Jaumann, P. Masson, G. Neukum, L. E. Nyquist, and M. H. Carr (2001), Geological processes and evolution, *Sci. Rev.*, *96*, 263–292.

Hynek, B. M., R. J. Phillips, and R. E. Arvidson (2003), Explosive volcanism in the Tharsis region: Global evidence in the Martian record, *J. Geophys. Res.*, *108*(E95111), doi:10.1029/2003JE002062.

Kite, E. S., I. Halevy, M. A. Kahre, M. J. Wolff, and M. Manga (2013), Seasonal melting and the formation of sedimentary rocks on Mars, with predictions for the Gale Crater mound, *Icarus*, *181-210*, 223, doi:10.1016/j.icarus.2012.11.034.
Komatsu, G., P. E. Geissler, R. G. Strom, and R. B. Singer (1993), Stratigraphy and erosional landforms of layered deposits in Valles Marineris, Mars, *J. Geophys. Res.*, *98*(E6), 11,105–11,121.
Komatsu, G., G. G. Ori, P. Ciarcelluti, and Y. D. Litasov (2004), Interior layered deposit of Valles Marineris, Mars: Analogous subice volcanism related to Baikal Rifting, Southern Siberia, *Planet. Space Sci.*, *52*, 167–187, doi:10.1016/j.pss.2003.08.003.
Laskar, J., A. C. M. Correia, M. Gastineau, F. Joutel, B. Levrarda, and P. Robutel (2005), Long term evolution and chaotic diffusion of the insolation quantities of Mars, *Icarus*, *170*, 343–364, doi:10.1016/j.icarus.2004.04.005.
Le Deit, L., et al. (2008), Ferric oxides in East Candor Chasma, Valles Marineris (Mars) inferred from analysis of OMEGA/Mars Express data: Identification and geological interpretation, *J. Geophys. Res.*, *113*, E07001, doi:10.1029/2007JE002950.
Le Deit, L., J. Flahaut, C. Quantin, E. Hauber, D. Mège, O. Bourgeois, J. Gurgurewicz, M. Massé, and R. Jaumann (2012), Extensive surface pedogenic alteration of the Martian Noachian crust suggested by plateau phyllosilicates around Valles Marineris, *J. Geophys. Res.*, *117*, E00J05, doi:10.1029/2011JE003983.
Lewis, K. W., O. Aharonson, J. P. Grotzinger, R. L. Kirk, A. S. McEwen, and T.-A. Suer (2008), Quasi-periodic bedding in the sedimentary rock record of Mars, *Science*, *322*(5907), 1532–1535, doi:10.1126/science.1161870.
Lucchitta, B. K. (1987), Recent mafic volcanism on Mars, *Science*, *235*, 565–567, doi:10.1126/science.235.4788.565.
Lucchitta, B. K. (1990), Young volcanic deposits in the Valles Marineris, Mars?, *Icarus*, *86*, 476–509, doi:10.1016/0019-1035(90)90230-7.
Lucchitta, B. K. (1999), Geologic map of Ophir and Central Candor Chasmata (MTM-05072) of Mars, U.S. Geological Map, I-2568.
Lucchitta, B. K. (2001), MOC images confirm layered deposits formed within Valles Marineris, Mars, Lunar Planet. Sci., XXXII, 1359.pdf.
Lucchitta, B. K. (2010), Lakes in Valles Marineris, in *Lakes on Mars*, edited by N. A. Cabrol and E. A. Grin, pp. 111, Elsevier, Amsterdam.
Lucchitta, B. K., and M. L. Bertolini (1990), Interior structures of Valles Marineris, Mars, *Lunar Planet. Sci.*, *XX*, 590–591.
Lucchitta, B. K., et al. (1992), The canyon system on Mars, in *Mars (A93-27852 09-91)*, pp. 453–492, The University of Arizona Press, Tucson and London.
Lucchitta, B. K., N. K. Isbell, and A. Howington-Kraus (1994), Topography of Valles Marineris: Implications for erosional and structural history, *J. Geophys. Res.*, *99*(E2), 3783–3798.
Madeleine, J. B., F. Forget, J. W. Head, B. Leyrard, F. Montmessin, and E. Millour (2009), Amazonian northern mid-latitude glaciation on Mars: A proposed climate scenario, *Icarus*, *203*, 390–405, doi:10.1016/j.icarus.2009.04.037.
Malin, M. C., and K. S. Edgett (2000), Sedimentary rocks of the early Mars, *Science*, *290*, 1927–1937.
Malin, M. C., and K. S. Edgett (2001), Mars Global Surveyor Mars Orbiter Camera: Interplanetary cruise through primary mission, *J. Geophys. Res.*, *106*(E10), 23,429–23,570, doi:10.1029/2000JE001455.
Malin, M. C., et al. (2007), Context Camera Investigation on board the Mars Reconnaissance Orbiter, *J. Geophys. Res.*, *112*, E05S04, doi:10.1029/2006JE002808.
Mangold, N., et al. (2008), Spectral and geological study of the sulfate-rich region of west Candor Chasma, Mars, *Icarus*, *194*(2), 519–543, doi:10.1016/j.icarus.2007.10.021.
Matthews, N. E., V. C. Smith, A. Costa, A. J. Durant, D. M. Pyle, and N. J. G. Pearce (2012), Ultra-distal tephra deposits from super-eruptions: Examples from Toba, Indonesia and Taupo Volcanic Zone, New Zealand, *Quat. Geochronol.*, *258*, 54–79, doi:10.1016/j.quaint.2011.07.010.
McEwen, A. S., et al. (2007), Mars Reconnaissance Orbiter's High Resolution Imaging Science Experiment (HiRISE), *J. Geophys. Res.*, *112*, E05S02, doi:10.1029/2005JE002605.
Mège, D. (2001), Uniformitarian plume tectonics: The post-Archean Earth and Mars, in *Mantle Plumes: Their Identification Through Time*, Spec. Pap. Geol. Soc. Am., vol. 352, edited by R. E. Ernst and K. L. Buchan, pp. 141–164, Geol. Soc. Am., Boulder, Colo.
Mège, D., and O. Bourgeois (2011), Equatorial glaciations on Mars revealed by gravitational collapse of Valles Marineris wallslopes, *Earth Planet. Sci. Lett.*, *310*, 182–191, doi:10.1016/j.epsl.2011.08.030.
Mège, D., and R. E. Ernst (2001), Contractional effects of mantle plumes on Earth, Mars, and Venus, in *Mantle Plumes: Their Identification Through Time*, Spec. Pap. Geol. Soc. Am., vol. 352, edited by R. E. Ernst and K. L. Buchan, pp. 103–140, Geol. Soc. Am., Boulder, Colo.
Mège, D., and P. Masson (1996), A plume tectonics model for the Tharsis province, Mars, *Planet. Space Sci.*, *44*(12), 1499–1546.
Moratto, Z. M., M. J. Broxton, R. A. Beyer, M. Lundy, and K. Husmann (2010), Ames Stereo Pipeline, NASA's Open Source Automated Stereogrammetry Software, Lunar Planet. Sci. XLI, Abstract #2364.
Murchie, S. L., et al. (2007), Compact reconnaissance imaging spectrometer for Mars (CRISM) on Mars Reconnaissance Orbiter (MRO), *J. Geophys. Res.*, *112*, E05S03, doi:10.1029/2006JE002682.
Murchie, S. L., et al. (2009a), A synthesis of Martian aqueous mineralogy after 1 Mars year of observations from the Mars Reconnaissance Orbiter, *J. Geophys. Res.*, *114*, E00D06, doi:10.1029/2009JE003342.
Murchie, S. L., et al. (2009b), Evidence for the origin of layered deposits in Candor Chasma, Mars from mineral composition and hydrologic modeling, *J. Geophys. Res.*, *114*, E00D05, doi:10.1029/2009JE003343.
Murchie, S. L., et al. (2009c), The compact reconnaissance imaging spectrometer for Mars investigation and data set from the Mars Reconnaissance Orbiter's primary science phase, *J. Geophys. Res.*, *114*, E00D07, doi:10.1029/2009JE003344.
Mustard, J. F., et al. (2008), Hydrated silicate minerals on Mars observed by the Mars Reconnaissance Orbiter CRISM instrument, *Nature*, *454*, 305–309.
Nedell, S. S., S. W. Squyres, and D. W. Andersen (1987), Origin and evolution of the layered deposits in the Valles Marineris, Mars, *Icarus*, *70*, 409–441.
Neukum, G., et al. (2004), HRSC: The High Resolution Stereo Camera of Mars Express, *Eur. Space Agency Spec. Publ.*, *1240*, 17–35.
Noe Dobrea, E. Z., J. J. Wray, F. J. Calef III, T. J. Parker, and S. L. Murchie (2012), Hydrated minerals on Endeavour Crater's rim and interior, and surrounding plains: New insights from CRISM data, *Geophys. Res. Lett.*, *39*, L23201, doi:10.1029/2012GL053180.
Okubo, C. (2010), Structural geology of Amazonian-aged layered sedimentary deposits in southwest Candor Chasma, Mars, *Icarus*, *207*, 210–225, doi:10.1016/j.icarus.2009.11.012.
Parente, M. (2008), A new approach to denoising CRISM images, Lunar Planet. Sci., XXXIX, Abstract #1391.
Pelkey, S. M., et al. (2007), CRISM multispectral summary products: Parameterizing mineral diversity on Mars from reflectance, *J. Geophys. Res.*, *112*, E08S14, doi:10.1029/2006JE002831.
Peterson, C. (1981), A secondary origin for the central plateau of Hebes Chasma, Proc. Lunar Planet. Sci., XI, 1459-1471.
Quantin, C., A. Gendrin, N. Mangold, J.-P. Bibring, F. Poulet, P. Allemand and the OMEGA Team (2005), Sulfate deposits identified by Omega in Melas Chasma, Lunar Planet. Sci., XXXVI, Abstract 1789.
Roach, L. H., J. F. Mustard, S. L. Murchie, J.-P. Bibring, F. Forget, K. W. Lewis, O. Aharonson, M. Vincendon, and J. L. Bishop (2009), Testing evidence of recent hydration state change in sulfates on Mars, *J. Geophys. Res.*, *114*, E00D02, doi:10.1029/2008JE003245.

Roach, L. H., J. F. Mustard, M. D. Lane, J. L. Bishop, and S. L. Murchie (2010), Diagenetic haematite and sulfate assemblages in Valles Marineris, *Icarus*, *207*(2), 659–674, doi:10.1016/j.icarus.2009.11.029.

Rossi, A. P., G. Neukum, M. Pondrelli, S. van Gasselt, T. Zegers, E. Hauber, A. Chicarro, and B. Foing (2008), Large-scale spring deposits on Mars?, *J. Geophys. Res.*, *113*, E08016, doi:10.1029/2007JE003062.

Schreiber, B. C., and M. E. Tabakh (2000), Deposition and early alteration of evaporites, *Sedimentology*, *47*, 215–238.

Schultz, R. A. (1998), Multiple-process origin of Valles Marineris basins and troughs, Mars, *Planet. Space Sci.*, *46*, 827–829, doi:10.1016/S0032-0633(98)00030-0.

Scott, D. H., and Tanaka, K. L. (1986), Geologic map of the western equatorial region of Mars, scale 1:15,000,000, U.S.G.S. Misc. Inv. Ser. Map I-1802-A.

Siegert, M. J., J. C. Ellis-Evans, M. Tranter, C. Mayer, J.-R. Petit, A. Salamatink, and J. C. Priscu (2001), Physical, chemical and biological processes in Lake Vostok and other Antarctic subglacial lakes, *Nature*, *414*, 603–609.

Spencer, R. J., and L. A. Hardie (1990), Control of seawater composition by mixing of river waters and midocean ridge hydrothermal brines, in *Fluid-Mineral Interactions: A tribute to H.P. Eugster, Saint-Louis*, Geochemical Society Special Publication 2, edited by R. J. Spencer and I. M. Chou, pp. 406–19, Geochem. Soc., San Antonio, Tex.

Squyres, S. W., D. W. Andersen, S. S. Nedell, and R. A. Wharton (1991), Lake Hoare, Antarctica: Sedimentation through a thick perennial ice cover, *Sedimentology*, *38*(2), 363–379.

Stack, K. M., and R. E. Milliken (2011), Reflectance spectroscopy of clay-sulfate mixtures: Implications for quantifying hydrated minerals and determining depositional environments on Mars, Lunar Planet. Sci. XLII, Abstract #2024.

Swayze, G. A. (1997), The hydrothermal and structural history of the Cuprite mining district, southwestern Nevada: An integrated geological and geophysical approach, ProQuest Dissertations And Theses; Thesis (PhD.)--University of Colorado at Boulder, 1997; Publication Number: AAI9725795; ISBN: 9780591348477; Source: Dissertation Abstracts International, Volume: 58-03, Section: B, page: 1176; 399 p.

Swithinbank, C. (1988), Satellite image atlas of glaciers of the world, Antarctica, United States Geological Survey Professional Paper 1386-B.

Tanaka, K. L. (1986), Proc. Lunar Planet. Sci., 17th, Part 1: The stratigraphy of Mars, *J. Geophys. Res.*, *91*(B13), E139–E158.

Warner, N. H., M. Sowe, S. Gupta, A. Dumke, and K. Goddard (2013), Fill and spill of giant lakes in the eastern Valles Marineris region of Mars, *Geology*, *41*, 675–678, doi:10.1130/G34172.1.

Weitz, C., M. Lane, M. Staid, and E. Dobrea (2008), Gray hematite distribution and formation in Ophir and Candor Chasmata, *J. Geophys. Res.*, *113*, E02016, doi:10.1029/2007JE002930.

Wentworth, S. J., E. K. Gibson, M. A. Velbel, and D. S. McKay (2005), Antarctic Dry Valleys and indigenous weathering in Mars meteorites: Implications for water and life on Mars, *Icarus*, *174*, 383–95.

Zegers, T. E., J. H. Oosthoek, A. P. Rossi, J. K. Blom, and S. Schumacher (2010), Melt and collapse of buried water ice: An alternative hypothesis for the formation of chaotic terrains on Mars, *Earth Planet. Sci. Lett.*, *297*(3–4), 496, doi:10.1016/j.epsl.2010.06.049.